AGU100 ADVANCING EARTH AND SPACE SCIENCE

JGR

Journal of Geophysical Research: Solid Earth

RESEARCH ARTICLE

10.1029/2017JB015364

Key Points:

- An inversion method of magnetic data in the presence of remanent magnetization is proposed
- Induced and remanent magnetizations are estimated for each block of the source domain, and corresponding magnetic anomalies are extracted
- Yeshan region (eastern China) is studied, where Cenozoic basalts were formed during a period of reversed direction of the geomagnetic field

Supporting Information:

- Supporting Information S1
- Data Set S1
- Data Set S2
- Data Set S3
- Data Set S4
- Data Set S5

Correspondence to:
X. Hu,
xyhu@cug.edu.cn

Citation:
Liu, S., Fedi, M., Hu, X., Baniamerian, J., Wei, B., Zhang, D., & Zhu, R. (2018). Extracting induced and remanent magnetizations from magnetic data modeling. *Journal of Geophysical Research: Solid Earth*, *123*. https://doi.org/10.1029/2017JB015364

Received 18 DEC 2017
Accepted 13 OCT 2018
Accepted article online 18 OCT 2018

Extracting Induced and Remanent Magnetizations From Magnetic Data Modeling

Shuang Liu[1,2,3], Maurizio Fedi[2], Xiangyun Hu[1], Jamaledin Baniamerian[2,4], Bangshun Wei[5], Dalian Zhang[5], and Rixiang Zhu[3]

[1]Hubei Subsurface Multi-Scale Imaging Key Laboratory, Institute of Geophysics and Geomatics, China University of Geosciences, Wuhan, China, [2]Department of Earth, Environmental and Resources Science, University of Naples Federico II, Naples, Italy, [3]State Key Laboratory of Lithospheric Evolution, Institute of Geology and Geophysics, Chinese Academy of Sciences, Beijing, China, [4]Department of Earth Sciences, College of Sciences and Modern Technologies, Graduate University of Advanced Technology, Kerman, Iran, [5]Geological Survey of Jiangsu Province, Nanjing, China

Abstract To investigate the crustal magnetic structure, it is important to assess the susceptibility and remanence properties of rocks and ores. In this paper, we propose a method to extract the contributions of induced and remanent magnetization from modeling of magnetic anomalies. We first estimate the direction of the total magnetization vector by studying the reduced-to-pole anomaly and its correlation with different magnitude magnetic transforms. Then we invert the magnetic data to obtain the volumetric distribution of the magnetization intensity. As the third step, based on a priori information about the Koenigsberger ratio derived from petrophysical measurements, we extract the distributions in the source volume of the induced and remanent magnetization intensities, based on a generalized relationship involving the total and remanent magnetizations, and the true susceptibility. In this way, we are able to produce separate maps of the anomaly fields attributed to the physical magnetic source parameters: remanent and induced magnetization. After validating the method with synthetic data, we analyze the data relative to the Mesozoic and Cenozoic igneous rocks in Yeshan region, eastern China. The analysis of the separated magnetization components reveals that the intrusion of dioritic and basaltic rocks occurred at different geological periods, and the basaltic rocks were magnetized by a reversed geomagnetic field. The uncertainty analysis shows that a larger Koenigsberger ratio is beneficial to extract more reliable remanence and susceptibility information.

1. Introduction

The natural remanent magnetization is an important component of the magnetic properties of rocks and ores. It contains information about Earth's magnetic field at the time the rocks and ores were formed or the time they underwent thermal and metamorphic processes. The remanent magnetization records the direction of the primary geomagnetic fields at different geologic ages, thereby providing critical evidence for many geological activities such as plate movement, seafloor spreading, and sedimentary evolution (e.g., Clark, 2014; Yang & Besse, 2001; Zhu et al., 1998). Hence, remanent magnetization is the fundamental physical parameter of paleomagnetic studies. However, because of the differences in formation conditions and subsequent geological events, estimation of the intensity and direction of remanent magnetization can be very complex.

Collecting oriented samples of rocks or ores and measuring their magnetic properties is the most common and accurate way to obtain the remanence strength and direction (Clark & Emerson, 1991). However, this is not possible when the target rocks are seriously weathered or covered by thick sediments. To overcome the problem of estimating the remanent magnetization and total magnetization of magnetic sources, many strategies have been proposed (Clark, 2014). For example, borehole measurements provide a way to obtain the susceptibility and remanence parameters; petrologic and paleomagnetic information can be used to infer probable remanence directions. However, most of these methods provide only partial information and have their strengths and weaknesses (Clark, 2014).

The total magnetization is the vectorial sum of the induced and remanent magnetizations. The direction of total magnetization can be estimated from the magnetic data. For example, Fedi et al. (1994) proposed the MAX-MIN method to calculate the magnetization direction from the reduced-to-pole (RTP) field computed at different directions of the magnetization vectors; Bilim and Ates (2004) estimated the total magnetization direction by determining the maximum correlation between pseudogravity and gravity anomalies. Phillips (2005) used Helbig's integrals to estimate the vector components of the magnetic dipole moment from the first-order moments of the vector magnetic field components. Nicolosi et al. (2006) computed the magnetization direction of crustal structures using an equivalent source algorithm. Dannemiller and Li (2006) estimated the total magnetization direction based on the correlation between the vertical gradient and the total gradient of the RTP field. Gerovska et al. (2009) obtained the magnetization direction by correlating the RTP field and magnitude transforms of magnetic anomalies. J. Li et al. (2017) estimated the magnetization direction of magnetic anomalies through correlation of normalized source strength (NSS) anomalies with the RTP field. Four of these methods will be tested in the current study and are described in more detail in the following section.

Additionally, inversion of magnetic data in the presence of remanence has been a subject of intense research in recent years, and many algorithms were implemented to deal with this issue. Some algorithms invert for amplitude anomalies, which are weakly sensitive to magnetization directions; these include the analytic signal (Shearer & Li, 2004; Srivastava & Agarwal, 2010), the magnitude magnetic anomaly (Leao-Santos et al., 2015; Y. Li et al., 2012, 2010; S. Li & Li, 2014; S. Liu et al., 2015), and the NSS (Beiki et al., 2012; Clark, 2012; Guo et al., 2014; Pilkington & Beiki, 2013; Zhou et al., 2015).

A different approach is the inversion of magnetic data to directly obtain the magnetization vector components. Wang et al. (2004) inverted the three components of total magnetization in a Cartesian framework. Lelièvre and Oldenburg (2009) presented an improved method that calculated the three magnetization components in a spherical framework, which serves more complicated scenarios and has widespread applicability in magnetic data inversion under the influence of significant remanent magnetization. Later, Ellis et al. (2012) defined the equations relating the magnetization components to the magnetic anomalies and then optimized the objective function to obtain the three components of the magnetization vector. S. Liu et al. (2013) inverted the 2-D magnetization vector distributions based on borehole magnitude magnetic anomalies. These studies were based on inversion of magnetic anomalies and focused on determining the geometry and position of the magnetic sources.

However, the methods mentioned above did not provide enough information to separate the remanent magnetization and true susceptibility from the total magnetization. This can be achieved if we have information on the Koenigsberger ratio, which describes the relative strength of the remanent and induced magnetization. Based on the Koenigsberger ratio we may use a generalized relationship between the total magnetization vector and the apparent susceptibility formulated by Fedi (1989) and further extract the intensity and direction of the remanence magnetization vector along with the true susceptibility. In our recent work, the remanence information was separated when we implemented the inversion of magnetic data with simultaneous significant remanent magnetization and self-demagnetization. (S. Liu et al., 2018).

This information is useful in a number of ways. First, the distribution of susceptibility and remanent magnetization can help reveal the geometry and depth of the magnetic sources, providing essential information for mineral resource exploration. Second, the values of the susceptibility and remanence are related to the magnetic mineral content. For example, pyrrhotite and hematite are associated mainly with remanence, whereas magnetite can carry remanence and susceptibility equally well. Different types of magnetization can provide information on the mineralogy. Finally, the extracted remanence direction provides information on past geological processes.

2. Methodology

2.1. Estimation of Total Magnetization Direction

Estimating the total magnetization direction is the first step of our method. As described above, there are many approaches to achieve this. However, the measured magnetic anomaly inevitably contains noise and these methods are not completely accurate; therefore, the estimated total magnetization direction always includes errors. In this study, multiple published methods are implemented and tested to increase the reliability of the estimated total magnetization direction.

Usually, the study of the RTP field or comparisons of RTP data with other transforms, which are weakly sensitive to the magnetization direction, are used to determine the magnetization direction. The magnitude magnetic anomaly (T_a) is a magnitude transform with low sensitivity to the magnetization direction and high centricity to magnetic sources (Gerovska & Araúzo-Bravo, 2006; Stavrev & Gerovska, 2000). In this regard, Gerovska et al. (2009) proposed the TA-RTP method to estimate the total magnetization direction through the correlation between the RTP field (T_{rtp}) and the magnitude magnetic anomaly

$$R = \Re\left(T_a, T_{\mathrm{rtp}}\right), \tag{1}$$

where R is the correlation coefficient between T_a and T_{rtp}; $\Re$ is the correlation operator given by

$$\Re = \frac{C_{i,j}}{\sqrt{C_{i,i} \cdot C_{j,j}}}, \tag{2}$$

and $C_{i,i}$, $C_{j,j}$, and $C_{i,j}$ are the covariance and cross-covariance between two variables of index i and j. Therefore, the optimal values of the inclination (I*) and declination (D*) of the magnetization are those for which the correlation coefficients of equation (1) are maximum:

$$[I^*, D^*] = \text{ arg max } R^{2N+1}(I, D), \tag{3}$$

where N is a positive integer used to enhance the maximum position of the correlation coefficient map.

The magnitude magnetic anomaly in equation (1) is not an ideal quantity to estimate the magnetization direction, because it still shows a weak sensitivity to the magnetization direction, particularly in the case of a nearly horizontal magnetization. The NSS (Beiki et al., 2012; Clark, 2012; Guo et al., 2014; Pilkington & Beiki, 2013; Zhou et al., 2015) was shown to be a superior transformation, showing less sensitivity to the magnetization direction than the magnitude magnetic anomaly or the analytic signal. J. Li et al. (2017) proposed to estimate the magnetization direction, based on their correlations (the NSS-RTP method), as expressed by

$$R = \Re\left(\mu, T_{\mathrm{rtp}}\right), \tag{4}$$

where μ is the NSS of the magnetic anomaly. Similar to equation (3), the magnetization direction corresponding to the maximum correlation is considered as the appropriate direction.

Instead of directly comparing different transforms with the RTP field, Dannemiller and Li (2006) proposed a method based on the correlation between the vertical gradient (T_{rtpz}) and the total gradient (T_{rtpt}) of the RTP field (the VG-TG method):

$$R = \Re\left(T_{\mathrm{rtpz}}, T_{\mathrm{rtpt}}\right). \tag{5}$$

A different approach was proposed by Fedi et al. (1994), who suggested estimating the maximum of the lows of a set of RTP fields computed for different inclinations and declinations of either the total or the induced magnetization vectors (the MAX-MIN method):

$$[I^*, D^*] = \text{ arg max}\left[\min T_{\mathrm{rtp}}(I, D)\right]. \tag{6}$$

This method found many applications in real examples of magnetization direction determination (e.g., Cordani & Shukowsky, 2009; Mantovani et al., 2016).

2.2. Inversion of Total Magnetization Intensity

We use regular discretization to invert the total magnetization intensity; the subsurface is divided into prismatic cells with every cell homogeneously magnetized. The relationship between the measured total field anomaly and the total magnetization intensity can be expressed as a linear matrix equation:

$$\mathbf{Gm} = \mathbf{d}, \tag{7}$$

where **m** is the model parameter vector of total magnetization intensity, **d** is the observed total field anomaly, and **G** is the ($m \times n$)-dimensional kernel matrix (m is the number of observed data and n is number of mesh cells).

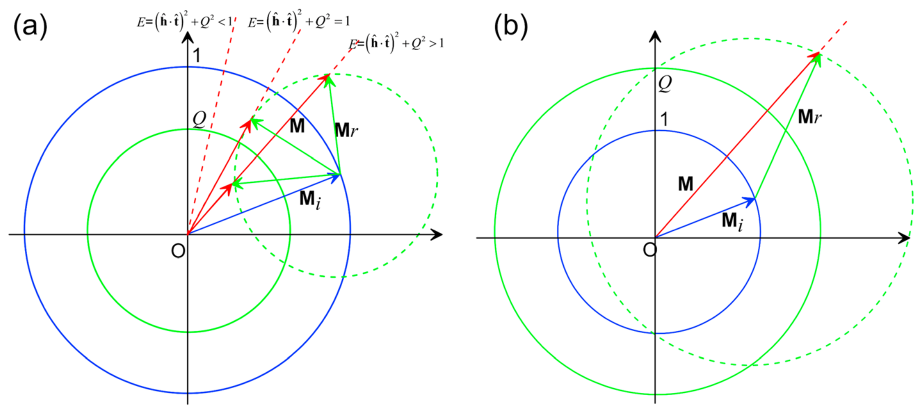

Figure 1. Sketch map of the relationships among total magnetization vector, induced magnetization vector, and remanent magnetization vector, when Koenigsberger ratio (a) $Q < 1$ and (b) $Q \geq 1$. When $Q \geq 1$, a unique remanence direction is obtained. If $Q < 1$ and $E > 1$, there will be two possible directions of remanent magnetization. The blue, green, and red arrows represent the induced, remanent, and total magnetizations, respectively. The blue circle represents the induced magnetizations of different directions with the same intensity. Similarly, the green circle represents the remanent magnetizations of different directions with the same intensity.

The objective function of regularization inversion for magnetic data is given by Y. Li and Oldenburg (1996, 1998)

$$\phi = \|\mathbf{W}_d(\mathbf{d} - \mathbf{Gm})\|_2^2 + \lambda\|\mathbf{W}_m(\mathbf{m} - \mathbf{m}_{\text{ref}})\|_2^2, \tag{8}$$

where ϕ is the objective function, λ is the regularization factor, $\mathbf{m}_{\text{ref}}$ is the reference model, and $\mathbf{W}_d$ and $\mathbf{W}_m$ are the data and model weighting matrices, respectively.

In this study, we wrote the code of preconditioned conjugate gradient algorithm (S. Liu et al., 2013; Pilkington, 1997) and carried out the inversion of total magnetization intensity.

2.3. Extraction of Remanent Magnetization and True Susceptibility From Total Magnetization Vector

The total magnetization vector is the vector sum of the induced and remanent magnetization vector (Figure 1):

$$\mathbf{M} = \mathbf{M}_i + \mathbf{M}_r = \kappa\mathbf{H}_0 + \mathbf{M}_r, \tag{9}$$

where $\mathbf{M}$ is the total magnetization vector, $\mathbf{M}_i$ is the induced magnetization vector, $\mathbf{M}_r$ is the remanent magnetization vector, κ is the magnetic susceptibility, and $\mathbf{H}_0$ is the geomagnetic field.

For a negligible remanent magnetization, the magnetic anomaly inversion yields the susceptibility distribution, which is equal to the total magnetization intensity divided by the geomagnetic field intensity. In this case, the Koenigsberger ratio (Q) (Clark & Emerson, 1991; Hinze et al., 2013)

$$Q = \frac{|\mathbf{M}_r|}{|\mathbf{M}_i|} = \frac{|\mathbf{M}_r|}{|\kappa\mathbf{H}_0|}, \tag{10}$$

is very low. If Q is high, combining equations (9) and (10), the apparent susceptibility (κa) is related to the true susceptibility (κ) by the following relationship, given by Fedi (1989):

$$\kappa_a = \kappa\left(1 + Q^2 + 2QC\right)^{1/2}. \tag{11}$$

The apparent susceptibility can be written as the ratio of magnetization intensity to geomagnetic field intensity:

$$\kappa_a = \frac{|\mathbf{M}|}{|\mathbf{H}_0|}. \tag{12}$$

Here C is related to the directions of the geomagnetic field and of the remanent magnetization:

$$C = \cos I_0 \cos I_r \cos(D_0 - D_r) + \sin I_0 \sin I_r, \tag{13}$$

and I_0, D_0, I_r, and D_r are the inclination and declination of the geomagnetic field (i.e., induced magnetization) and remanent magnetization, respectively. Equation (11) needs to satisfy

$$F = Q^2 + 2QC \geq -1. \tag{14}$$

Moreover, based on equations (9) and (10), we may obtain a relationship among the directions of total magnetization, remanent magnetization, and induced magnetization (Clark, 2014; Cordell & Taylor, 1971; Fedi, 1989):

$$\widehat{\mathbf{m}} = \begin{cases} \frac{1}{Q}\left[(a+b)\widehat{\mathbf{t}} - \widehat{\mathbf{h}}\right] & (Q \geq 1) \\ \frac{1}{Q}\left[(a \pm b)\widehat{\mathbf{t}} - \widehat{\mathbf{h}}\right] & (Q < 1) \end{cases}, \tag{15}$$

where a and b are

$$\begin{cases} a = \widehat{\mathbf{h}} \cdot \widehat{\mathbf{t}} = \cos\theta \\ b = \left[\left(\widehat{\mathbf{h}} \cdot \widehat{\mathbf{t}}\right)^2 - 1 + Q^2\right]^{1/2} \end{cases}, \tag{16}$$

and $\widehat{\mathbf{m}}$, $\widehat{\mathbf{t}}$, and $\widehat{\mathbf{h}}$ are the unit vectors of the remanent magnetization, total magnetization, and induced magnetization, respectively; θ is the angle between the total magnetization and the geomagnetic field. Equations (15) and (16) are required to satisfy

$$E = \left(\widehat{\mathbf{h}} \cdot \widehat{\mathbf{t}}\right)^2 + Q^2 \geq 1. \tag{17}$$

Equation (15) indicates that if Q is known as a priori information, the remanence direction can be determined from the directions of the total magnetization and induced magnetization (i.e., the geomagnetic field direction).

Equation (15) also demonstrates that two solutions are possible when $Q < 1$ and $E > 1$. As shown in Figure 1a, there are two intersection points between the remanence (green circle) and the total magnetization (red arrow). The blue circle displays the induced magnetization. If $Q < 1$ and $E < 1$, the remanent magnetization does not have a solution. When $Q \geq 1$, the green circle always intersects the red arrow at one point, which corresponds to the unique solution of the remanence direction (Figure 1b).

In summary, the process of separating the susceptibility and remanent magnetization contributions from the inverted magnetic data is based on the following steps.

a) Estimate the direction of total magnetization (equations (1), (4), (5), and (6)).
b) Compute the direction of the remanent magnetization (equation (15)).
c) Invert the total magnetization intensity for each block (*Steps b* and *c* can be interchanged).
d) Compute the true susceptibility for each block (equations (11) and (12)).
e) Compute the intensity of the remanent magnetization (equation (10)).

3. Synthetic Examples

3.1. Synthetic Model

We analyzed the case of a synthetic magnetic model, namely a homogeneously magnetized prism with its center located at (x_0, y_0, z_0) = (500 m, 500 m, 500 m) and sides of lengths a = 100 m, b = 200 m, and c = 200 m (Table S1 in the supporting information). Four values were used for the Koenigsberger ratio: Q = 0, 0.2, 1, and

10.1029/2017JB015364

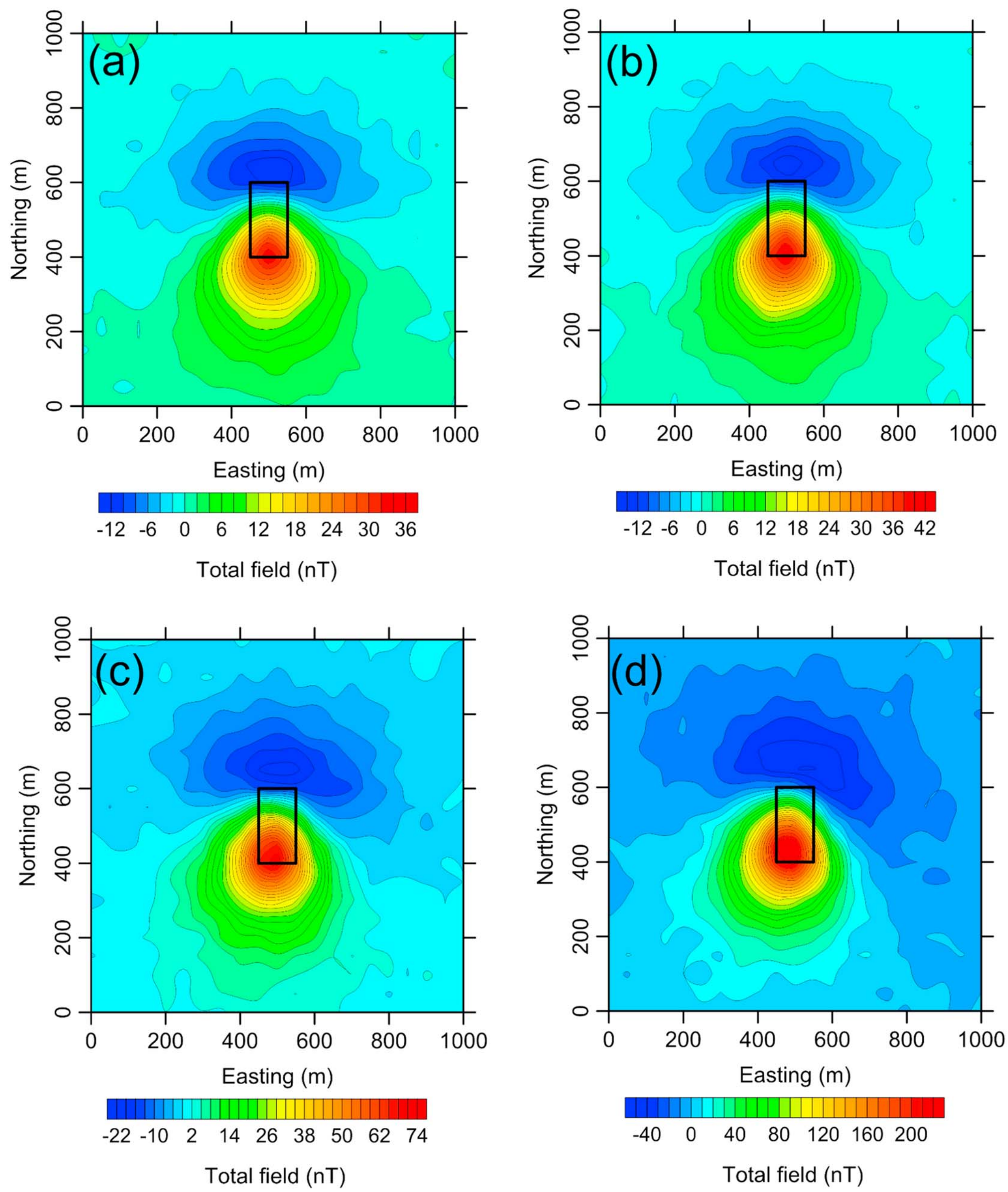

Figure 2. Total field anomalies of the synthetic prism model with different remanent magnetization intensities of Koenigsberger ratio (a) $Q = 0$, (b) $Q = 0.2$, (c) $Q = 1$, and (d) $Q = 5$. Zero-mean Gaussian noises with standard deviation = 0.5, 0.6, 1, and 3 nT are added to the magnetic data in Figures 2a–2d, respectively. The susceptibility of prism $\kappa = 0.0126$ SI and geomagnetic intensity, inclination, and declination are $T_0 = 50{,}000$ nT, $I_0 = 45°$, and $D_0 = 0°$. The inclination and declination of remanent magnetization are $I_r = 60°$ and $D_r = 60°$.

5. For all four cases, the susceptibility is 0.0126 SI, and the inclination and declination of the remanent magnetization are both equal to 60°. The geomagnetic field intensity was assumed to be T_0 = 50,000 nT with inclination I_0 = 45° (horizontal to downward) and declination D_0 = 0° (north). The data grid was 50 × 50 m, with 21 × 21 = 441 observation points. Zero-mean Gaussian noise with standard deviations = 0.5, 0.6, 1, and 3 nT was added to the magnetic data of the four cases (Q = 0, 0.2, 1, and 5), respectively. The different noise levels for the different test scenarios were chosen to scale the noise to the overall magnetic anomalies. Thus, we can regard the noisy total field anomalies in Figure 2 as realistic synthetic data, provided the Koenigsberger ratios (Q = 0, 0.2, 1, and 5) are known as a priori information.

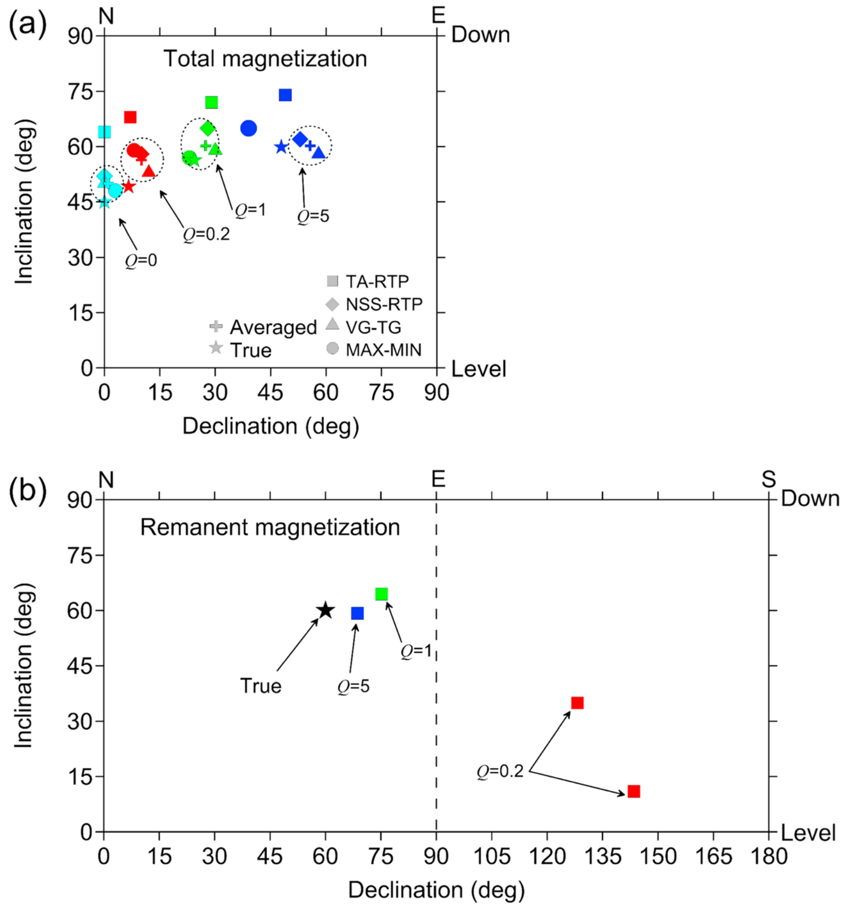

Figure 3. (a) The estimated total magnetization directions using TA-RTP, NSS-RTP, VG-TG, and MAX-MIN and (b) the extracted remanent magnetization directions for the synthetic models in Figure 2. When $Q = 0.2$, two remanence directions are obtained and they have large differences with the true values. When $Q = 1$, the inclination and declination of remanence have errors about 5° and 15°, respectively. When $Q = 5$, it returns the same inclination as the true values and the declination yields a solution having an error about 8°.

3.2. Estimating the Directions of the Total Magnetization and of the Remanent Magnetization

In the first step we used the TA-RTP, NSS-RTP, VG-TG, and MAX-MIN methods to estimate the total magnetization direction (*Step a*). The inclination and declination were increased from 0° to 90° in 1° steps. The contour maps of the correlation coefficients ($N = 10$ in equation (3)) and the minimum RTP value clearly show the maximum points, which correspond to the optimal total magnetization directions (Figure S1).

Table S2 lists all the estimated directions of total magnetization for the four cases using the TA-RTP, NSS-RTP, VG-TG, and MAX-MIN methods. A comparison of these estimates with the true values indicates that NSS-RTP, VG-TG, and MAX-MIN returned more stable and accurate total magnetization directions than TA-RTP, with an average error (i.e., the difference between the derived and true values) of less than 10°. TA-RTP returned accurate declinations, but its inclination errors reach 15–20° (Table S2).

To increase the accuracy and the reliability of the total magnetization direction estimation, we used the average values of the clustered solutions (within the dashed lines in Figure 3a) as the final total magnetization direction. In this example, the solutions of the TA-RTP method and MAX-MIN method for the $Q = 5$ case were abandoned. Finally, compared with the true values, the averaged total magnetization directions for the four cases yielded errors less than 8° (Table S2).

Based on the estimated total magnetization directions, the remanent magnetization directions were calculated by using equation (15) (*Step b*, Figure 3b and Table S2). When $Q = 0.2$, two groups of remanence directions were estimated, but the results are incorrect when compared with the true values. This occurred because the computation of the remanent magnetization direction is unstable for low Koenigsberger ratios (i.e., $Q < 1$) as described in more detail below. In the case of $Q = 1$, the solution improved and the final inclination and declination have errors of about 5° and 15°, respectively (Table S2). When $Q = 5$, the inclination estimates are similar to the true values, with a 1° precision, and the declination estimate yielded an acceptable solution having a small error of about 8° (Table S2).

3.3. Separating Susceptibility and Remanent Magnetization From the Total Magnetization Vector

Y. Li et al. (2010) pointed out that the inversion yields inaccurate results if the error of the given total magnetization direction exceeds 15°. If we consider this criterion, we may accept the estimated average directions of the total magnetization direction in Figure 3a and Table S2. Using these estimates, we developed the code of the preconditioned conjugate gradient algorithm (S. Liu et al., 2013; Pilkington, 1997) to invert for the total magnetization intensity (*Step c*) and then compute for each block the true susceptibility (*Step d*) and the intensity of the remanent magnetization (*Step e*). The subsurface was divided into cubic cells with a 25-m side length; the number of cells was $40 \times 40 \times 20 = 32{,}000$. Figure 4 shows the results of the inverted total magnetization intensity and the extracted susceptibility and remanent magnetization, for different Koenigsberger ratios. There is no remanence to be recovered when $Q = 0$.

For the four cases $Q = 0$, 0.2, 1, and 5, the recovered intensity values of the total magnetization, susceptibility, and remanent magnetization are consistent with the true values (Figure 4 and Table S1). The cross sections of magnetization intensity distributions show that the shapes and depths of the recovered model are acceptable; however, because the total magnetization direction used in the calculations is only an approximation with a considerable uncertainty and true error of 8°, the recovered models shows a slightly southerly dip (Figure 4). In addition, as the susceptibility and remanence have the same sources and the Koenigsberger ratio of the sources is uniform, the distributions of the total magnetization, remanence, and susceptibility have a similar pattern, and only differences in their intensities are observed.

In summary, this method is able to extract the susceptibility and remanence, including its intensity and direction, based on a priori information for the Koenigsberger ratio. The precision of the estimated remanence and susceptibility is related to that of the estimated total magnetization direction and to the a priori information of the Koenigsberger ratio. When $Q < 1$, the process of extracting the remanence direction is unstable and two possible solutions can be obtained; a priori geological information can help choose the correct solution. The computations of the susceptibility and intensity of the remanence show a stable process in this example. In general, the more accurate the Koenigsberger ratio and total magnetization direction, the higher the reliability of the remanence and susceptibility results.

4. Uncertainty Analysis

4.1. Uncertainty Analysis of the Remanent Magnetization Direction Extraction

The synthetic examples demonstrate that the differences in the remanent magnetization direction between the estimated and true values increase with decreasing Koenigsberger ratio (Figure 3b and Table S2). Equation (15) reveals that the error of computing the remanence direction is attributed to the error in the estimation of the total magnetization direction and in the a priori information of the Koenigsberger ratio. Based on equation (15), therefore, we can define the partial derivative of $\widehat{\mathbf{m}}$ with respect to the two parameters. For $\widehat{\mathbf{t}}$, we obtain the sensitivity factor S_t:

$$S_t = \frac{\partial \widehat{\mathbf{m}}}{\partial \widehat{\mathbf{t}}} = \begin{cases} \frac{1}{Q}\left(2a + b + a^2 b^{-1}\right) & (Q \geq 1) \\ \frac{1}{Q}\left(2a \pm b \pm a^2 b^{-1}\right) & (Q < 1) \end{cases}, \tag{18}$$

where a and b are the parameters in equation (16). Similarly, the partial derivative of $\widehat{\mathbf{m}}$ with respect to Q is given by

$$\mathbf{S}_Q = \frac{\partial \widehat{\mathbf{m}}}{\partial Q} = \begin{cases} -\frac{\widehat{\mathbf{m}}}{Q} + \frac{\widehat{\mathbf{t}}}{b} & (Q \geq 1) \\ -\frac{\widehat{\mathbf{m}}}{Q} \pm \frac{\widehat{\mathbf{t}}}{b} & (Q < 1) \end{cases}, \tag{19}$$

whose modulus is defined as the sensitivity factor to the Koenigsberger ratio. Therefore,

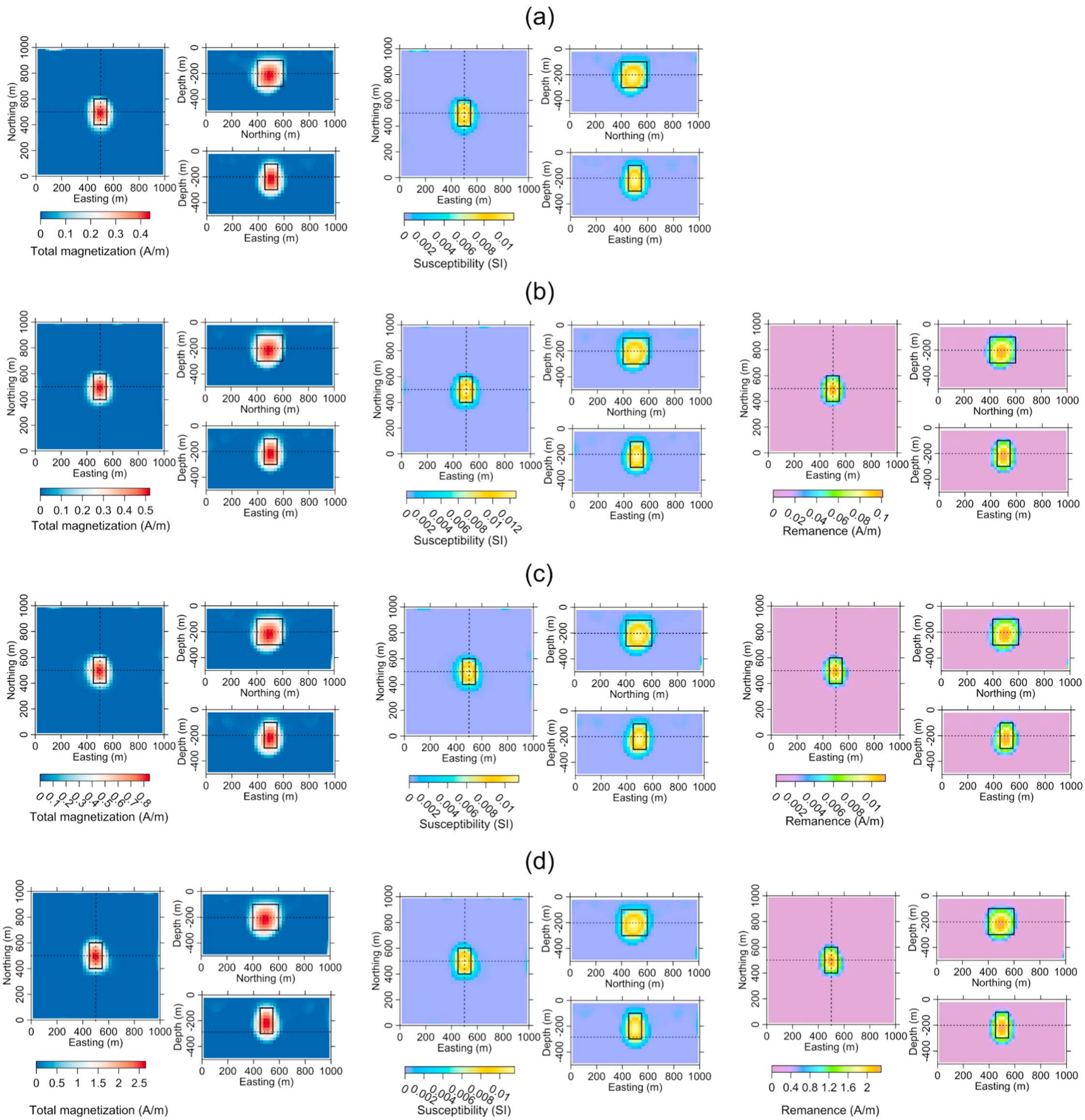

Figure 4. Horizontal and vertical cross sections of the inverted total magnetization intensity, remanent magnetization, and susceptibility for the synthetic models in Figure 2 for (a) $Q = 0$, (b) $Q = 0.2$, (c) $Q = 1$, and (d) $Q = 5$. The magnitudes, shapes, and depths of the recovered total magnetization, susceptibility, and remanent magnetization are consistent with the true models.

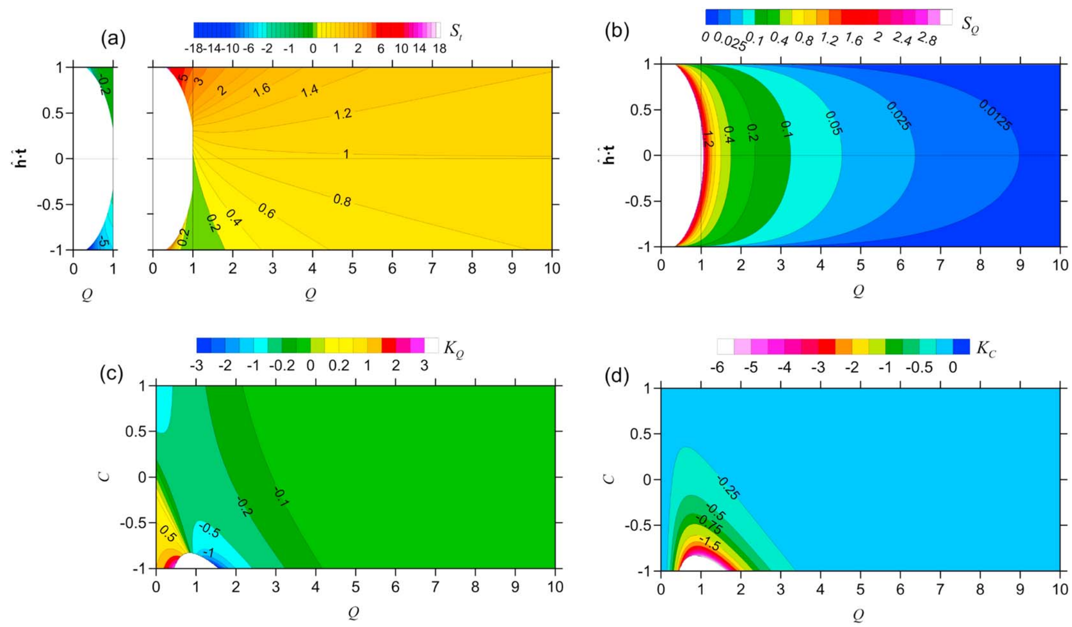

Figure 5. Sensitivity factors of the remanent magnetization direction with respect to (a) total magnetization direction and (b) Koenigsberger ratio; and sensitivity factors of susceptibility and remanent magnetization intensity with respect to (c) Koenigsberger ratio and (d) remanent magnetization direction. Areas of blanks and large values indicate the no-solution and unstable regions.

$$S_Q = |\mathbf{S}_Q| = \left(\frac{1}{b^2} - \frac{1}{Q^2}\right)^{1/2} \quad (Q \geq 1, Q < 1), \tag{20}$$

The reliability of the computed remanent magnetization direction can be evaluated by the sensitivity factors S_t and S_Q. If the errors in the total magnetization direction and a priori Koenigsberger ratio are assumed to be $\mathbf{e}_t$ and e_Q, respectively, the propagated errors in the remanent magnetization direction are given by

$$\begin{cases} \mathbf{e}_{mt} = S_t \mathbf{e}_t \\ \mathbf{e}_{mQ} = \mathbf{S}_Q e_Q \end{cases}, \tag{21}$$

where $\mathbf{e}_{mt}$ and $\mathbf{e}_{mQ}$ are the errors in the estimation of the remanent magnetization direction. Therefore, $S_t > 1$ and $S_Q > 1$ indicate amplified errors.

Figure 5a and 5b shows the sensitivity factors S_t and S_Q. As shown in equation (15), there are two possible directions for the remanent magnetization when $Q < 1$; correspondingly, the sensitivity analysis for $Q < 1$ also includes two parts (equation (18) and Figure 5a). Generally, the S_t map shows three unstable regions for $Q < 1$: $\left(\widehat{\mathbf{h}} \cdot \widehat{\mathbf{t}}\right)^2 + Q^2 \rightarrow 1$, $\widehat{\mathbf{h}} \cdot \widehat{\mathbf{t}} \rightarrow -1$, and $\widehat{\mathbf{h}} \cdot \widehat{\mathbf{t}} \rightarrow 1$, in which the errors of total magnetization are enlarged dramatically. Here $\widehat{\mathbf{h}} \cdot \widehat{\mathbf{t}} = \pm 1$ indicates that they are in the same and opposite directions. When $Q > 1$ then $S_t < 3$, and the computational process is stable (Figure 5a). For S_Q, when $\left(\widehat{\mathbf{h}} \cdot \widehat{\mathbf{t}}\right)^2 + Q^2 \rightarrow 1$, $S_Q \rightarrow +\infty$, indicating the unstable regions. In other regions, S_Q has small values (Figure 5b).

In the synthetic example, for $Q = 0.2$, the TA-RTP, NSS-RTP, and MAX-MIN methods do not produce solutions because their E values are less than 1. For the VG-TG method, $E > 1$, but $|S_t| >> 1$ and $|S_Q| >> 1$ (Table S3), so that the extracted remanence direction is unstable and has a large error (Figure 3b and Table S2). When $Q = 1$ and 5, $S_t < 4$, and $S_Q < 0.4$ (Table S3), the solutions are stable and acceptable.

4.2. Uncertainty Analysis of the Remanent Magnetization Intensity and Susceptibility Extraction

Equation (11) reveals that the errors from the Koenigsberger ratios and remanent magnetization directions will also affect the final results of the susceptibility and remanent magnetization intensity. Similarly, the following quantities

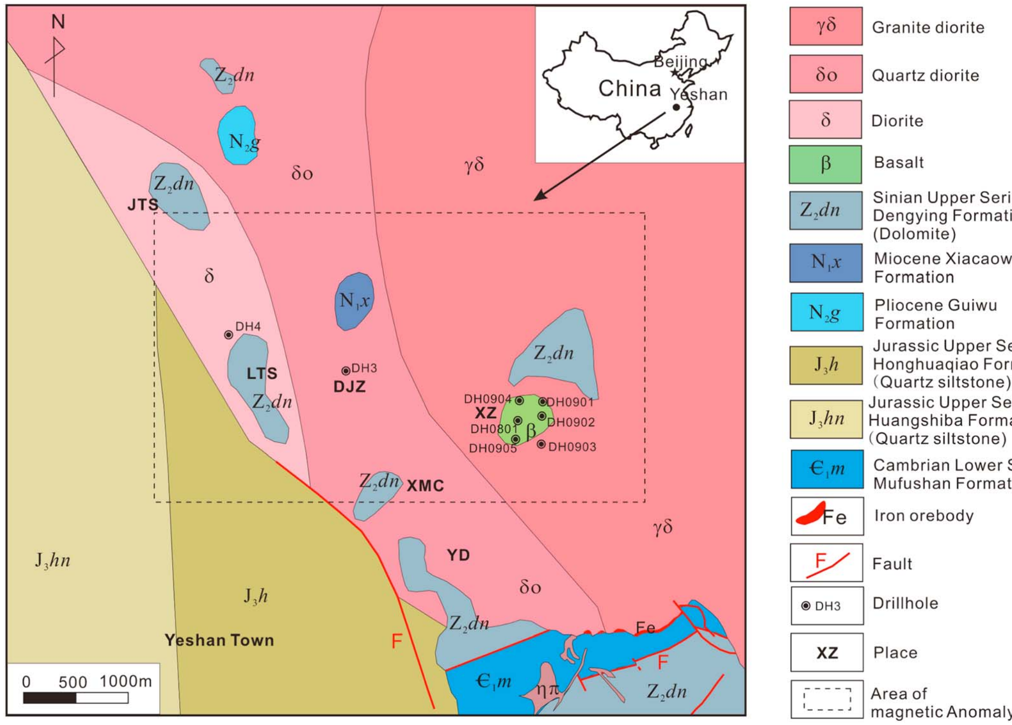

Figure 6. Geological map of the Yeshan region. Late Yanshanian intrusive rocks are outcropping in this area. LTS = Laitoushan; DJZ = Dajingzhao; XZ = Xuezhuang; JTS = Jiutoushan; XMC = Xiaomiaochen; YD = Yaodun.The dashed box shows the outline of Figure 7.

$$\begin{cases} K_Q = \dfrac{\partial}{\partial Q}\left(\dfrac{\kappa}{\kappa_a}\right) = -(Q+C)\left(1+Q^2+2QC\right)^{-3/2} \\ K_C = \dfrac{\partial}{\partial C}\left(\dfrac{\kappa}{\kappa_a}\right) = -Q\left(1+Q^2+2QC\right)^{-3/2} \end{cases}, \tag{22}$$

describe the stability of computing the susceptibility and remanent magnetization, where $0 \leq C \leq 1$ (equation (13)).

Equation (22) implies that there is no solution at the range $F = Q^2 + 2QC < -1$, and that computations of the susceptibility and remanent magnetization will not be stable if $F \rightarrow -1$. As shown in Figures 5c and 5d, the amplitudes of K_Q and K_C are much larger than 1 in the areas of $-1 \leq C \leq -0.8$ and $0 \leq Q \leq 2$, indicating instability of the computational processes. Conversely, low values of K_Q and K_C indicate good stability for the computation of the values of the susceptibility and remanence. In the synthetic examples, all the methods for estimating the total magnetization direction yield small K_Q and K_C, with values always less than 1 (Table S3). Therefore, as concluded from Figure 4, the inversion of the remanent magnetization and the susceptibility of the synthetic example are stable.

5. Field Example: Extracting Remanent Magnetization and Susceptibility Information for the Mesozoic and Cenozoic Igneous Rocks of the Yeshan Region (Eastern China)

5.1. Geological and Geophysical Data Sets

The Yeshan region (118.9°E, 32.5°N) comprises an important polymetallic deposit in Jiangsu province, eastern China, which is located in the northeastern part of the Yangtze block (Zheng et al., 2013). The exposed sedimentary rocks in this area are mainly dolomite and limestone of the upper Sinian and lower Cambrian age. The late Yanshanina intrusive rocks are also widely distributed (Figure 6, Zhang et al., 2016). The mineralization processes are related to the intrusive rocks of moderate-acidic diorite, granite diorite, and

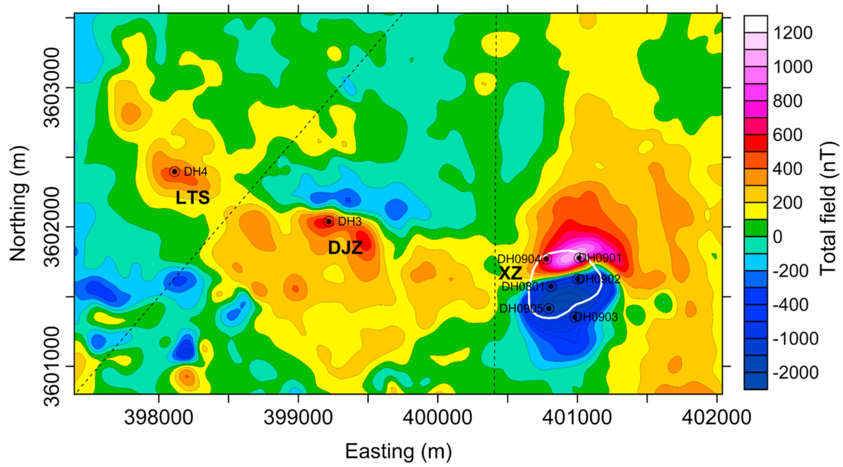

Figure 7. Total field anomaly and drill hole positions of the Yeshan region (eastern China). The white curve shows the boundary of the basalt rocks outcropping in XZ area. Black points show the position of drill holes. LTS = Laitoushan; DJZ = Dajingzhao; XZ = Xuezhuang. Dash lines show the regions of LTS, DJZ, and XZ.

quartz diorite. However, the three-dimensional geometry and depth features of these igneous rocks are unknown. More evidence needs to be provided to investigate the patterns and ages of the magmatic intrusions. Studying the relationship between the magmatic intrusions and mineralization is still a challenge in this area (Zhang et al., 2016).

The ground total field magnetic anomalies show three main anomalous areas: Laitoushan (LTS), Dajingzhao (DJZ), and Xuezhuang (XZ, Figure 7). The anomaly at LTS is positive, with an amplitude of 300 nT, while DJZ shows a dipole character with the highest amplitude reaching 600 nT. The most eastern anomaly (XZ) shows a reverse dipole signature whose amplitude varies from −2,100 to 1,200 nT. Several boreholes, mostly less than 100-m deep, were drilled in the area to prospect shallow ore bodies, mostly at depths of less than 100 m (Figure 7). The deepest borehole DH4 (526-m deep) is located in the LTS and crosses the quartz-diorite, monzonite-diorite, dioritic porphyrite, and syenite rocks. DH3 is located in DJZ, and the core was mainly diorite, dioritic porphyrite, and (biotite) monzonite. Other boreholes in XZ were drilled through thick basalts. Drilled core has revealed the rock types, and a large number of magnetic properties are measured (Table S4). In particular, the Koenigsberger ratios were determined, including those of basalt (~5.7) and dioritic porphyrite (~4.3). Alterated syenite, granodiorite, and monzonite have Koenigsberger ratios in the range of 0.5–1.2. Unfortunately, there are no oriented samples from these areas and the direction of the respective remanent magnetization is still unknown. In the Yeshan region, the geomagnetic field intensity is T_0 = 49,997 nT, with inclination I_0 = 49.1° and declination D_0 = −5.6°.

5.2. Results of the Remanence and Susceptibility Extraction

The patterns of the LTS, DJZ, and XZ anomalies indicate that the total magnetization directions of each anomaly are different. Therefore, we first use the TA-RTP, NSS-RTP, VG-TG, and MAX-MIN methods to estimate their directions. The inclinations range from −90° to 90° in 1° intervals, and the declinations range from −180° to 180° in 1° intervals. The correlation maxima (equation (3), N = 5) and the RTP minima correspond to the optimal directions of total magnetization (Figure S2). The MAX-MIN method did not clearly locate the maxima in LTS and DJZ because of high noise levels in the observed magnetic data. The MAX-MIN result of the XZ anomaly and the TA-RTP result of the DJZ anomaly deviate significantly from the other clustered direction; therefore, these two results were also not used to estimate the remanent magnetization direction.

The uncertainty of the estimated total magnetization direction is usually determined from the contour map of the correlation coefficient by defining an area with, for example, 90% of the maximum correlation coefficient. However, this is not a convenient way when using four different methods; moreover, being different from the other methods, MAX-MIN is not based on the correlation coefficient to estimate the total magnetization direction. Therefore, in this study we determined the final total magnetization direction and its uncertainty by analyzing the clustering characteristics of the solutions from the different methods. From

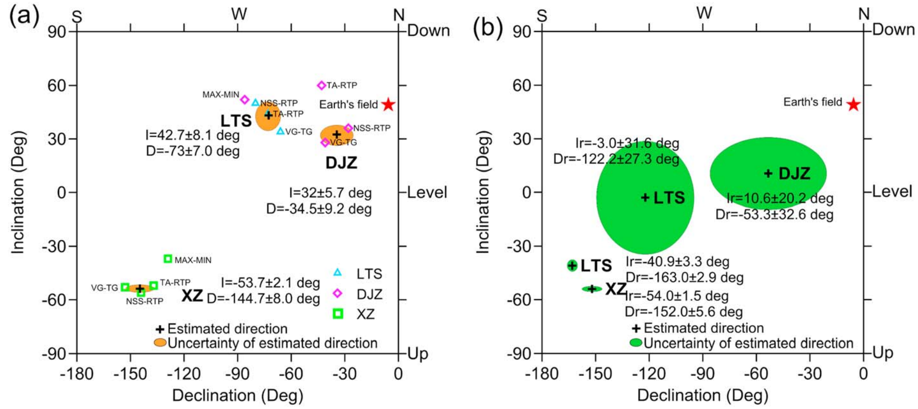

Figure 8. Computed directions of (a) total magnetization and (b) remanent magnetization of the LTS, DJZ, and XZ areas at Yeshan region (eastern China). Two remanence directions are obtained in LTS. Remanent magnetization in DJZ points north-west. Remanent magnetization in XZ lies in southwestern and upward oriented. The remanence direction in XZ has high reliability with uncertainty <5.6° based on the estimated error of the total magnetization direction. The respective uncertainty is about 20–30° for DJZ and one of the solutions of LTS. LTS = Laitoushan; DJZ = Dajingzhao; XZ = Xuezhuang.

the remaining solutions (three for LTS, three for DJZ, and two for XZ), we considered the average final direction for each area. Their standard deviations describe the uncertainty ranges of the estimated magnetization directions. The estimated inclination and declination of the total magnetization in the three regions are (1) LTS: I = 42.7 ± 8.1°; D = 73 ± 7.0°; (2) DJZ: I = 32 ± 5.7°; D = −34.5 ± 9.2°; and (3) XZ: I = −53.7 ± 2.1°; D = −144.7 ± 8.0° (Figure 8a and Table S5). The evaluated scatter for all three domains was <10°, which is less than the 15° error threshold given by Y. Li et al. (2010).

The error of remanence direction extraction is determined by the uncertainties in total magnetization direction estimation and in Koenigsberger ratio measurement. The total uncertainty is equal to the sum of the uncertainties from the total magnetization direction and the Koenigsberger ratio because the two effects can be regarded as approximately independent. In this study, therefore, we evaluated these two factors separately to better understand the reliability of the results.

Based on the estimated total magnetization direction and its uncertainty (Figure 8a), the directions of the remanent magnetization were finally determined as (1) LTS: Ir = −3.1 ± 31.6°, Dr = −122 ± 27.3°; Ir = −40.9 ± 3.3°, Dr = −163 ± 2.9°; (2) DJZ: Ir = 10.6 ± 20.2°, Dr = −53.3 ± 32.6°; and (3) XZ: Ir = −54.0 ± 1.5°, Dr = −152 ± 5.6° (Figure 8b and Table S5). For the LTS anomaly, because the Koenigsberger ratio is less than 1, two different directions were obtained. The remanent magnetization in the DJZ area points north-west. The direction of the remanent magnetization in the XZ area is south-west and upward oriented, which is reversed with respect to the current geomagnetic field. Additionally, the remanence direction in XZ has high reliability with an uncertainty of <5.6°. However, in DJZ and one of the solutions of LTS, the uncertainties reached 20–30° because of the large uncertainty in the total magnetization direction estimation. The small Koenigsberger ratio further amplifies the errors (Figure 8b).

In LTS, the average Koenigsberger ratios for alterated diorite, alterated syenite, granodiorite, and monzonite varied from 0.5 to 1.2 (Table S4). Alterated syenite and granodiorite, the main rocks of the DJZ area, have average Koenigsberger ratios of 0.6 and 1.2, respectively. Measurement of the physical properties of more than 100 basalt samples revealed that the basalt has strong remanence with a 5.7 average Koenigsberger ratio. To sum up and to simplify, we chose their average values as the final Koenigsberger ratios with an uncertainty of ±20%. Thus, the Koenigsberger ratios of the LTS, DJZ, and XZ anomalies were set as Q = 0.8 ± 0.16, Q = 1.0 ± 0.2, and Q = 5.7 ± 1.14, respectively (Figure 9a). In XZ, the ±20% uncertainty of Koenigsberger ratio has a weak influence (< 2%) on the remanence results, while in LTS and DJZ the ±20% error in the Koenigsberger ratio will produce errors of 5–15% in the remanence direction (Figure 9b). In addition, it is noticeable that the uncertainty areas of the LTS and DJZ are comprised two parts because there are possible remanence directions when Q < 1 (see equation (18)).

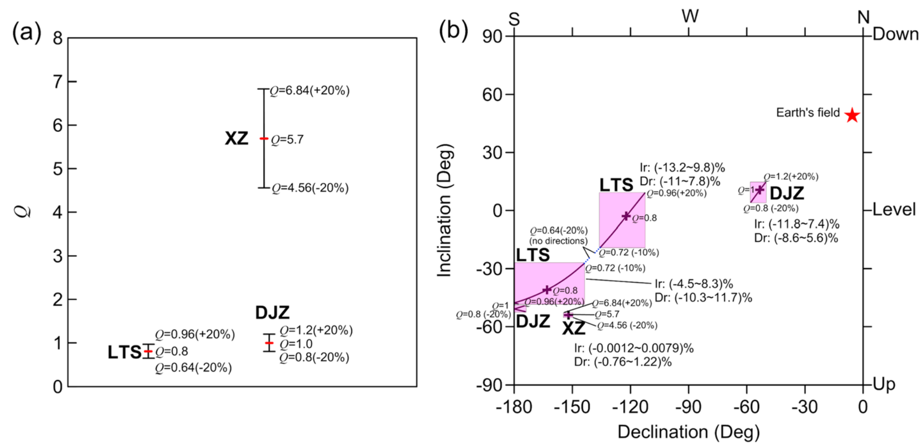

Figure 9. Uncertainty analysis of (a) Koenigsberger ratio errors to the (b) estimated remanent magnetization directions of the LTS, DJZ, and XZ areas at Yeshan region (eastern China). In XZ, a ± 20% uncertainty of Koenigsberger ratio has low influences (<2%) on the remanence results. In LTS and DJZ, ±20% of Koenigsberger ratio errors produce 5–15% errors for remanence directions. LTS = Laitoushan; DJZ = Dajingzhao; XZ = Xuezhuang.

Once the directions of total magnetization and remanent magnetization are estimated, we can recover the three-dimensional distributions of the total magnetization, remanent magnetization, and susceptibility. The whole area is divided into three sections (LTS, DJZ, and XZ; Figure 7); each one is the same area as used for determining the total magnetization direction. The subsurface is divided into 794,880 (184 × 108 × 40) cubes with 25-m side length. A constraint of positive magnetization intensity and susceptibility is considered in the inversion processes. Figure 10a shows the isosurface plot of the recovered total magnetization intensity distributions, which is greater than 1.5 A/m for LTS and DJZ, and greater than 4 A/m for XZ. Figure 10b shows the separated remanent magnetization isosurface plot; the intensity is greater than 1.2 A/m for LTS and DJZ and greater than 5 A/m for XZ. Figure 10c presents the isosurface plot of the susceptibility, which is greater than 0.03 SI in all three areas.

Figure 11 illustrates the cross sections of the reconstructed total magnetization intensity, remanent magnetization, and susceptibility across boreholes DH4, DH3 and DH0901, DH0902, and DH0903. The magnetic sources for the three regions are different. The LTS anomaly is caused by variations of diorites; the DJZ source is composed of diorite, diorite-porphyrite, and monzonite, and the reversed magnetic anomaly observed in XZ is attributed to basalt rocks. The inversion results show that all the intrusions extend to several hundred meters depth and that the LTS rocks dip north, while the DJZ rocks tend to dip south. The basalt rocks in XZ are vertically intruded.

After separating the different components of magnetization, the corresponding magnetic anomalies can be calculated. Figures 12a–12c shows the observed and modeled anomalies of the total magnetization inversion and the difference between them, respectively. A deviation between the two data sets is notable in XZ, where a background anomaly of about 200 nT appears. The induced magnetic anomalies vary from −250 to 450 nT with fairly the same amplitudes in XZ, LTS, and DJZ (Figure 12d), while the magnetic anomaly due to only the remanent magnetization component is more intense at XZ than at LTS and DJZ (Figure 12e). The total field anomaly responses attributed to the induced and remanent magnetizations are quite different.

5.3. Discussion

According to the above data processing and inversion, we obtained the distributions of the total magnetization intensity, remanent magnetization, and susceptibility, as well as the corresponding magnetization directions and magnetic anomalies of the LTS, DJZ, and XZ areas. This information helps to determine the geometries and positions of these intrusion rocks and provides evidence for the geological interpretation of these igneous rocks.

In LTS, DJZ, and XZ areas, the mineral types and compositions of each rock are nearly the same (Y. Li et al., 2016). Thus, the Koenigsberger ratio for each rock was given by a constant value. This assumption and simplicity led to the phenomenon that the distributions of total magnetization intensity, remanent

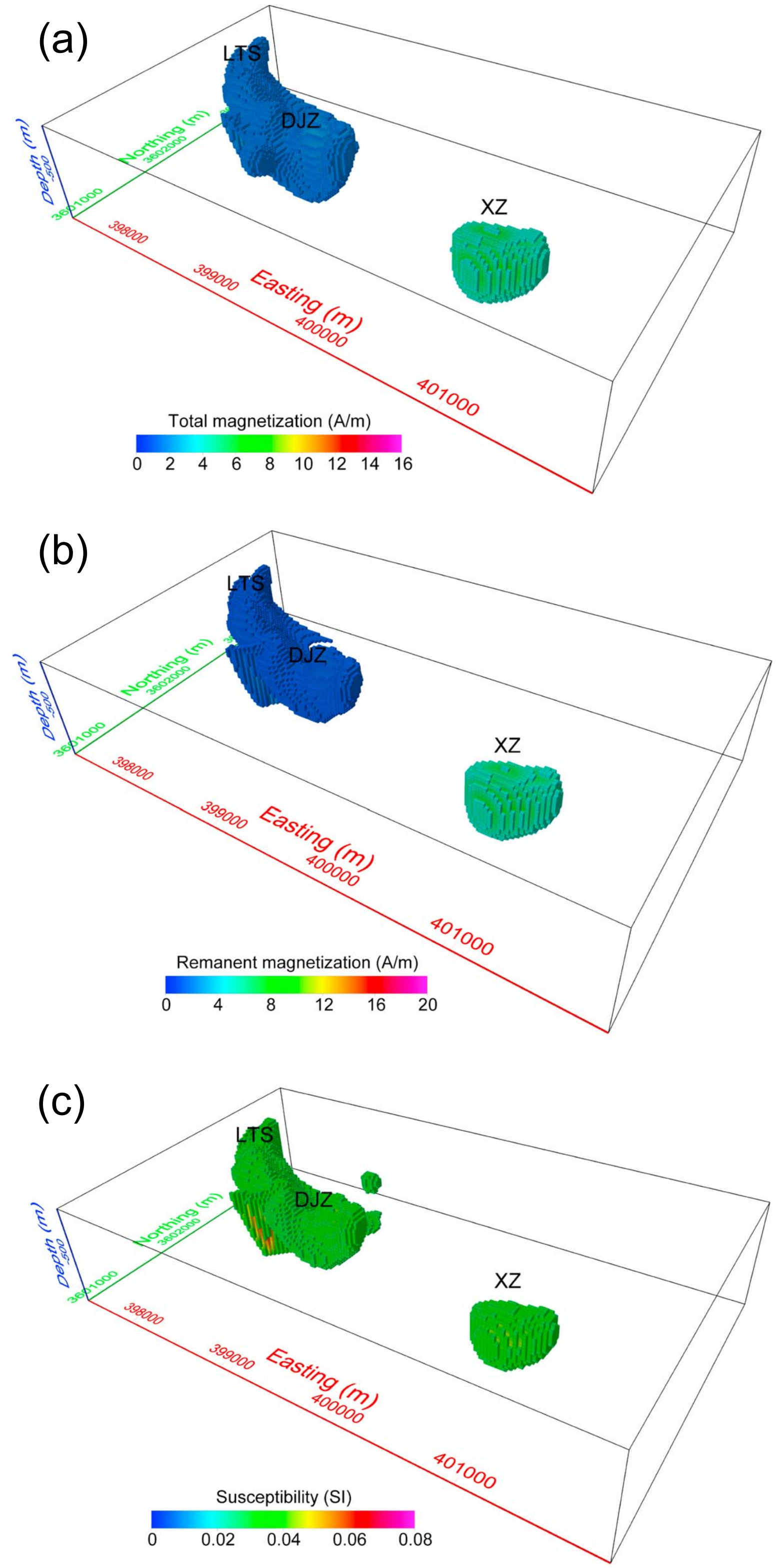

Figure 10. Isosurface plots of the inverted (a) total magnetization intensity (> 1.5 A/m at LTS and DJZ; > 4 A/m at XZ), (b) remanent magnetization (> 1.2 A/m at LTS and DJZ; > 5 A/m at XZ), and (c) susceptibility (> 0.03 SI at LTS, DJZ, and XZ) in the Yeshan region (eastern China). XZ rocks show higher total magnetization and remanent magnetization than those of LTS and DJZ. All three areas have the similar susceptibility magnitude. LTS = Laitoushan; DJZ = Dajingzhao; XZ = Xuezhuang.

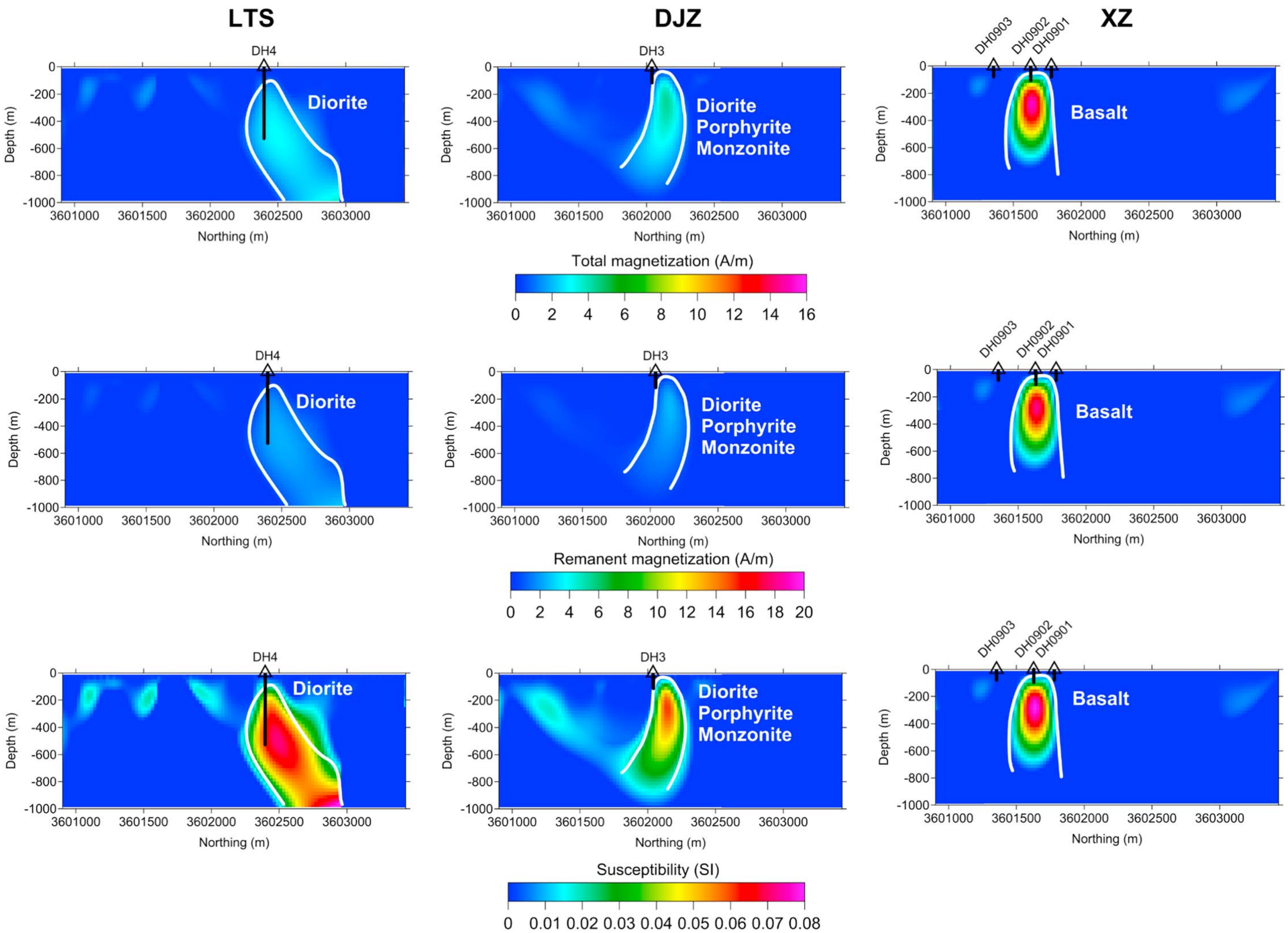

Figure 11. Drill holes and reconstructed magnetic sources from the inverted total magnetization intensity (top row), remanent magnetization (middle row), and susceptibility (bottom row) of the LTS (left column), DJZ (middle column), and XZ (right column) areas at Yeshan region (eastern China). The white curves display the approximate boundaries of the magnetic sources based on the inverted magnetization and susceptibility distributions. The inversion results show that the LTS rocks dip north, while DJZ rocks tend to dip south. The basalt rocks in XZ are vertically intruded. LTS = Laitoushan; DJZ = Dajingzhao; XZ = Xuezhuang.

magnetization, and susceptibility for each rock showed a similar shape both in the isosurface and cross-section plots (Figures 10 and 11), because their ratios also maintain constant. For the complex cases that have spatially varying Koenigsberger ratios, we can obtain the different distributions of total magnetization intensity, remanent magnetization, and susceptibility.

The extracted remanent magnetization and susceptibility in Figures 10 and 11 indicate that the LTS, DJZ, and XZ rocks have the same susceptibility but different remanent magnetization intensities. XZ rock shows 4–5 times higher remanent magnetization than LTS and DJZ rocks. Generally, the remanent magnetization of a rock depends on its material constituents, geological origin, and historical geomagnetic field (Clark, 1997; Q. Liu, 2011). The petrology and geochemistry data from Y. Li et al. (2016) revealed that the Cenozoic basalts in Yeshan region are rich in iron-titanium oxides (TiO_2: 2–3 wt %, Fe_2O_{3T}: 11–13 wt %) and are cryptocrystalline or microcrystalline texture, which may be the reason that XZ basalt rocks show strong remanent magnetization.

In the LTS area, the estimated inclination and declination of the total magnetization contain a 7–8° error using various methods. Since the Koenigsberger ratio is less than 1 (i.e., $Q < 1$), two possible directions of remanent magnetization are computed. One is horizontal, and the other is reversed with respect to the current

10.1029/2017JB015364

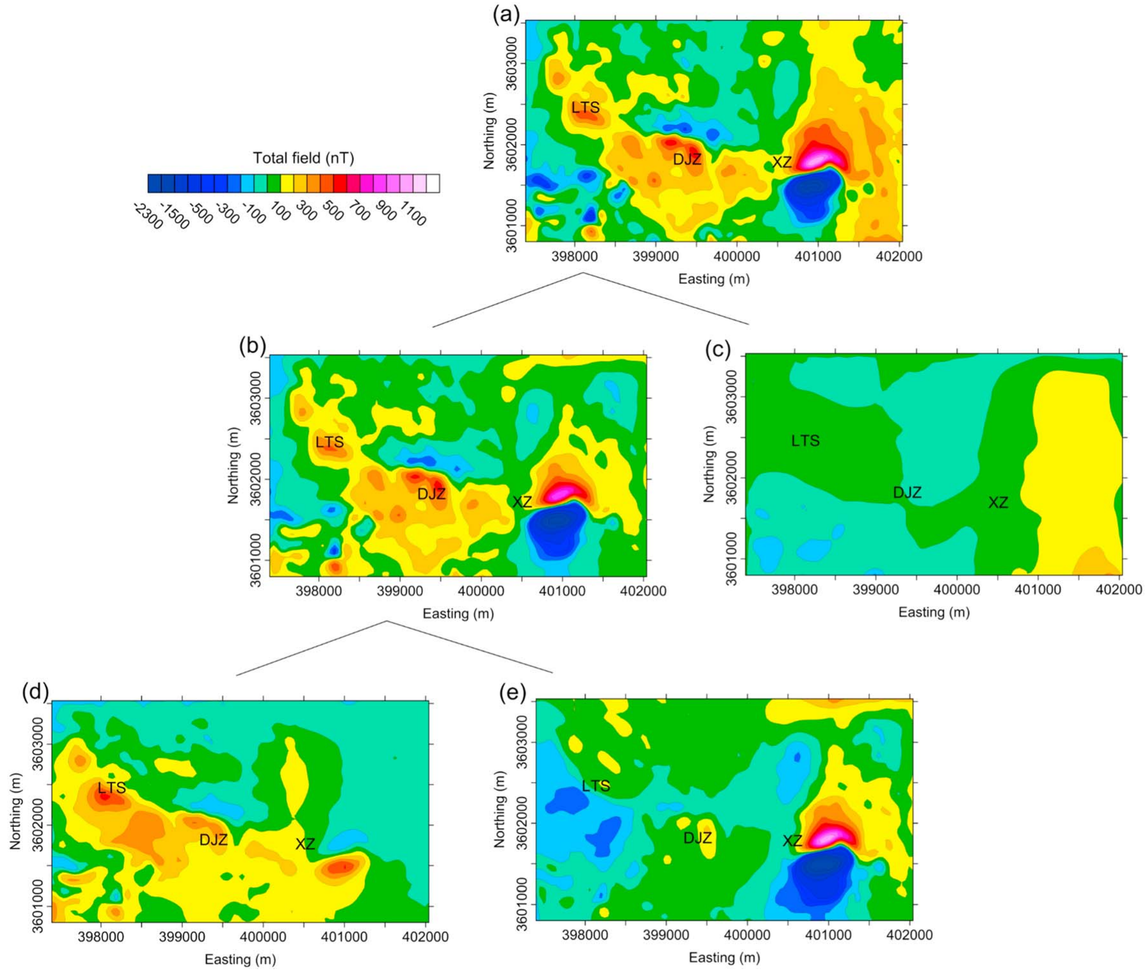

Figure 12. (a) Observed total field anomaly, (b) modeled total field anomaly, and (c) misfit (i.e., observed-modeled) for the total magnetization intensity inversion; the separated total field anomalies caused by (d) induced magnetization only and (e) remanent magnetization only. LTS = Laitoushan; DJZ = Dajingzhao; XZ = Xuezhuang.

geomagnetic field. These two solutions have different sensitivities (S_t and S_Q) to the total magnetization directions; hence, they do not have the same level of error. However, the latter solution will lead to high values of K_Q (= 3.7849) and K_C (= −19.9485), meaning that the computations of remanent magnetization intensity and susceptibility are unstable. For example, if we use this remanent magnetization direction to calculate the remanent magnetization, the intensity will reach 3 A/m, which disagrees with the physical property measurements (Table S4). Therefore, we chose the former solution as the final directions of total and remanent magnetization in the LTS area. For the DJZ and XZ anomalies, $Q \geq 1$ so that a unique remanent magnetization direction was calculated. Table S5 shows the computed directions of the total magnetization and remanent magnetization, and the sensitivity parameters. Overall, the XZ anomaly yielded the most accurate results because this area has the highest Koenigsberger ratio (Q = 5.7). For LTS and DJZ Q is close to 1, which leads to a large uncertainty in the estimate of the total magnetization direction.

Based on the information obtained of the remanent magnetization directions, the virtual geomagnetic poles (VGP) of the LTS, DJZ, and XZ areas can be calculated (Table S6 and Figure 13). The latitude and longitude of the VGP positions are LTS, $\lambda_p = 27.3°$, $\varphi_p = 226.7°$ and DJZ, $\lambda_p = 33.2°$, $\varphi_p = 371.4°$. The petrologic information reveals that the diorite and granodiorite rocks in LTS and DJZ were formed during the late Yanshanian period of the Mesozoic (116 Ma, normal geomagnetic polarity) (Y. Li et al., 2016). From the late Yanshanian period, the Yangtze block and the VGP are basically located at stable position and has small motions and rotations, with movement basically less than 10° (Wu et al., 1998; Zhu et al., 1998). The plate motion and geomagnetic

10.1029/2017JB015364

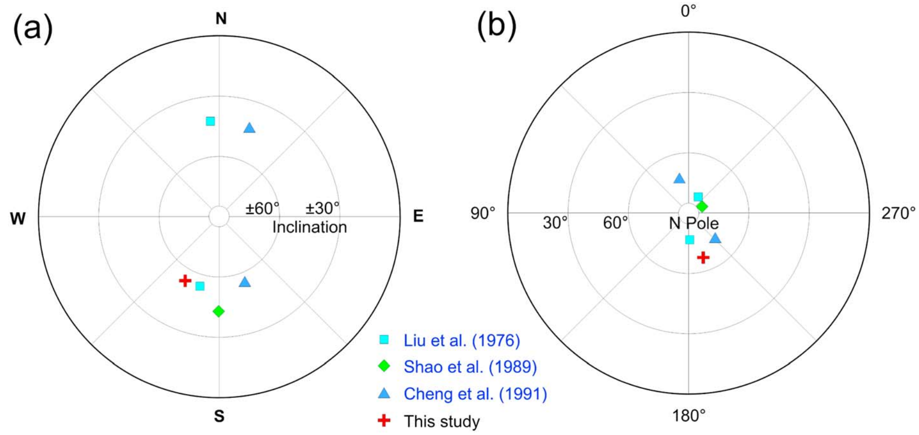

Figure 13. Comparison of (a) remanent magnetization directions and (b) virtual geomagnetic poles (VGP) for the basalt rocks of the XZ area, as estimated in this study and by previous work. XZ = Xuezhuang.

pole movement have a limited influence on the direction of remanent magnetization. So the computed VGP positions have large differences with real VGP position of Mesozoic, which is not attributed to the geologic events and plate motion.

The diorite and syenite in LTS and DJZ are alterated because they have undergone some metamorphism including the intrusion of basalt rocks of the XZ area. This metamorphism may have caused the change of remanent magnetization direction, so that the computed VGP positions may be different from the real VGP position in the Mesozoic (Wu et al., 1998; Zhu et al., 1998). However, because the metamorphism processes are complex and multistage, it is still difficult to analyze the specific metamorphic processes that alter their directions. For the XZ basalt rocks, the VGP (reversed polarity) is located at $\lambda_p = 66.8°$, $\varphi_p = 198.4°$. The intrusion of the basalt rocks in the XZ area occurred during a geomagnetic reversal, that is, the Pliocene and Miocene of late Tertiary (2.48–23.3 Ma) (Y. Li et al., 2016).

Cenozoic basalt is widely distributed throughout the XZ area and other regions of eastern China. Several authors implemented a paleomagnetism study based on the collected samples of these Cenozoic basalts (Cheng et al., 1991; C. Liu et al., 1976; Shao et al., 1989). Figure 13 and Table S6 compare the direction of remanent magnetization and VGP results of other authors with the ones of this study. Our results are in good agreement with the paleomagnetic findings in the Fangshan area by C. Liu et al. (1976) and Cheng et al. (1991). The geomagnetic polarity of the XZ basalt is reversed, while the other nearby basalts were formed at a normal geomagnetic polarity age, such as in the Lingyansan (C. Liu et al., 1976) and Pingshan (Cheng et al., 1991) areas.

6. Conclusions

We first estimated the direction of the total magnetization by combining a number of existing methods (the MAX-MIN method and correlation methods between the RTP fields and magnitude magnetic transforms that are less sensitive to magnetization direction). Then the total magnetization intensity was inverted, and finally, the spatial distributions of the total magnetization vector were obtained. We used the generalized relationships among the total magnetization, induced magnetization, and remanent magnetization and the a priori information of the Koenigsberger ratio. On this basis, we extracted the intensity and direction of the total and remanent magnetization and the susceptibility and evaluated the related magnetic anomaly responses. However, as Q is assumed constant in each lithology, the same distributions of total magnetization intensity, remanence intensity, and susceptibility for this lithology are obtained. In reality, complex cases of spatially varying Q exist; therefore, we would like to continue this work in the future to expand the applicability of this methodology.

The computational processes involved in estimating the direction and intensity of magnetic remanence and the susceptibility are not entirely stable. Generally, the best results are obtained with large Koenigsberger ratios ($Q \geq 1$). When $Q \leq 1$, the computed errors may be amplified, leading to unstable remanence direction and intensity estimations. The level of instability depends on the physical relationships between the remanence, induced, and total magnetizations. The sensitivity parameters S_t, S_Q, K_Q, and K_C are used to assess the stability of the results. In general, larger Koenigsberger ratios are beneficial to extract more reliable remanence and susceptibility information.

The extraction of the remanent and induced magnetization and the computation of their specifically related magnetic field components may provide critical information for the interpretation of the magnetic sources' shapes and depth, as well as of the geological history. In the field examples of Yeshan region (eastern China), the remanent magnetization information was extracted, showing that the diorite and granite-diorite rocks in LTS and DJZ and the basalt rocks of the XZ area formed at different geologic periods and were subsequently reversely magnetized. The geological interpretation and the position and geometry of these intrusive rocks were verified by petrological, paleomagnetic, and borehole information. We note that the results from the TS and DJZ regions contain high uncertainties; therefore, the final subsurface model derived for these two regions should be viewed with caution. However, the method shows very stable and reliable results in the XZ region.

Acknowledgments
We gratefully acknowledge the Associate Editor Max Moorkamp, the reviewer Sofie Gradmann, and an anonymous reviewer for their constructive comments and suggestions that significantly improved the manuscript. We thank Qingsheng Liu, Tao Yang, Yanqing Li, Zhiyong Li, and Shihu Li for their helpful discussions. This study is supported by the National Key R&D Program of China (grant 2016YFC0600109), the National Natural Sciences Foundation of China (41604087 and 41874122), and the Fundamental Research Funds for the Central Universities, China University of Geosciences (Wuhan) (CUGL170407) during the postdoc of the first author at the University of Naples Federico II. Magnetic data of the synthetic and field examples can be found in the supporting information.

References

Beiki, M., Clark, D. A., Austin, J. R., & Foss, C. A. (2012). Estimating source location using normalized magnetic source strength calculated from magnetic gradient tensor data. *Geophysics*, *77*(6), J23–J37. https://doi.org/10.1190/geo2011-0437.1

Bilim, F., & Ates, A. (2004). An enhanced method for estimation of body magnetization direction from pseudogravity and gravity data. *Computers & Geosciences*, *30*(2), 161–171. https://doi.org/10.1016/j.cageo.2003.09.003

Cheng, G., Sun, Y., & Li, S. (1991). China paleomagnetic data list for Cenozoic. *Seismology and Geology*, *13*(2), 184–186. (in Chinese with English abstract)

Clark, D. (1997). Magnetic petrophysics and magnetic petrology: Aids to geological interpretation of magnetic surveys. *AGSO Journal of Australian Geology and Geophysics*, *17*, 83–104.

Clark, D. A. (2012). New methods for interpretation of magnetic vector and gradient tensor data I: Eigenvector analysis and the normalised source strength. *Exploration Geophysics*, *43*(4), 267–282.

Clark, D. A. (2014). Methods for determining remanent and total magnetisations of magnetic sources—A review. *Exploration Geophysics*, *45*(4), 271–304. https://doi.org/10.1071/EG14013

Clark, D. A., & Emerson, D. W. (1991). Notes on rock magnetization characteristics in applied geophysical studies. *Exploration Geophysics*, *22*(3), 547–555. https://doi.org/10.1071/EG991547

Cordani, R., & Shukowsky, W. (2009). Virtual Pole from Magnetic Anomaly (VPMA): A procedure to estimate the age of a rock from its magnetic anomaly only. *Journal of Applied Geophysics*, *69*(2), 96–102. https://doi.org/10.1016/j.jappgeo.2009.07.001

Cordell, L., & Taylor, P. T. (1971). Investigation of magnetization and density of a North Atlantic seamount using Poisson's theorem. *Geophysics*, *36*(5), 919–937. https://doi.org/10.1190/1.1440224

Dannemiller, N., & Li, Y. (2006). A new method for determination of magnetization direction. *Geophysics*, *71*(6), L69–L73. https://doi.org/10.1190/1.2356116

Ellis, R. G., B. de Wet, & I. N. Macleod (2012), Inversion of magnetic data for remanent and induced sources, *22nd ASEG International Geophysical Conference and Exhibition Extended Abstracts*, 1–4.

Fedi, M. (1989). On the interpretation of magnetic anomalies for strong remanent magnetizations. *Pure and Applied Geophysics*, *130*(4), 721–733. https://doi.org/10.1007/BF00881607

Fedi, M., Florio, G., & Rapolla, A. (1994). A method to estimate the total magnetization direction from a distortion analysis of magnetic anomalies. *Geophysical Prospecting*, *42*(3), 261–274. https://doi.org/10.1111/j.1365-2478.1994.tb00209.x

Gerovska, D., & Araúzo-Bravo, M. J. (2006). Calculation of magnitude magnetic transforms with high centricity and low dependence on the magnetization vector direction. *Geophysics*, *71*(5), I21–I30. https://doi.org/10.1190/1.2335516

Gerovska, D., Araúzo-Bravo, M. J., & Stavrev, P. (2009). Estimating the magnetization direction of sources from southeast Bulgaria through correlation between reduced-to-the-pole and total magnitude anomalies. *Geophysical Prospecting*, *57*(4), 491–505. https://doi.org/10.1111/j.1365-2478.2008.00761.x

Guo, L., Meng, X., & Zhang, G. (2014). Three-dimensional correlation imaging for total amplitude magnetic anomaly and normalized source strength in the presence of strong remanent magnetization. *Journal of Applied Geophysics*, *111*, 121–128. https://doi.org/10.1016/j.jappgeo.2014.10.007

Hinze, W. J., Von Frese, R. R., & Saad, A. H. (2013). *Gravity and magnetic exploration: Principles, practices, and applications*. New York: Cambridge University Press. https://doi.org/10.1017/CBO9780511843129

Leao-Santos, M., Li, Y., & Moraes, R. (2015). Application of 3D magnetic amplitude inversion to iron oxide-copper-gold deposits at low magnetic latitudes: A case study from Carajas Mineral Province, Brazil. *Geophysics*, *80*(2), B13–B22. https://doi.org/10.1190/geo2014-0082.1

Lelièvre, P. G., & Oldenburg, D. W. (2009). A 3D total magnetization inversion applicable when significant, complicated remanence is present. *Geophysics*, *74*(3), L21–L30. https://doi.org/10.1190/1.3103249

Li, J., Zhang, Y., Yin, G., Fan, H., & Li, Z. (2017). An approach for estimating the magnetization direction of magnetic anomalies. *Journal of Applied Geophysics*, *137*, 1–7. https://doi.org/10.1016/j.jappgeo.2016.12.009

Li, S., & Li, Y. (2014). Inversion of magnetic anomaly on rugged observation surface in the presence of strong remanent magnetization. *Geophysics*, *79*(2), J11–J19. https://doi.org/10.1190/geo2013-0126.1

Li, Y., He, Z. X., & Liu, Y. X. (2012). Application of magnetic amplitude inversion in exploration for volcanic units in a basin environment. *Geophysics*, *77*(5), B219–B225. https://doi.org/10.1190/geo2012-0008.1

Li, Y., Ma, C., & Robinson, P. T. (2016). Petrology and geochemistry of Cenozoic intra-plate basalts in east-central China: Constraints on recycling of an oceanic slab in the source region. *Lithos*, *262*, 27–43. https://doi.org/10.1016/j.lithos.2016.06.012

Li, Y., & Oldenburg, D. W. (1996). 3-D inversion of magnetic data. *Geophysics*, *61*(2), 394–408. https://doi.org/10.1190/1.1443968

Li, Y., & Oldenburg, D. W. (1998). 3-D inversion of gravity data. *Geophysics*, *63*(1), 109–119. https://doi.org/10.1190/1.1444302

Li, Y., Shearer, S. E., Haney, M. M., & Dannemiller, N. (2010). Comprehensive approaches to 3D inversion of magnetic data affected by remanent magnetization. *Geophysics*, *75*(1), L1–L11. https://doi.org/10.1190/1.3294766

Liu, C., Cheng, G., Ye, S., Zhu, X., Lin, J., & Li, S. (1976). The paleomagnetic study on some Cainozoic basalt groups in vicinity of Nanking and the preliminary determination of its geological ages. *Acta Geophysica Sinica*, *19*(2), 125–137. (in Chinese with English abstract)

Liu, Q. (2011). Why are Q-ratios high in the Sulu UHP metamorphic rocks? *Journal of Earth Science*, *22*(1), 115–116. https://doi.org/10.1007/s12583-011-0161-1

Liu, S., Fedi, M., Hu, X., Ou, Y., Baniamerian, J., Zuo, B., et al. (2018). Three-dimensional inversion of magnetic data in the simultaneous presence of significant remanent magnetization and self-demagnetization: Example from Daye iron-ore deposit, Hubei province, China. *Geophysical Journal International*, *215*(1), 614–634. https://doi.org/10.1093/gji/ggy299

Liu, S., Hu, X., Liu, T., Feng, J., Gao, W., & Qiu, L. (2013). Magnetization vector imaging for borehole magnetic data based on magnitude magnetic anomaly. *Geophysics*, *78*(6), D429–D444. https://doi.org/10.1190/geo2012-0454.1

Liu, S., Hu, X., Xi, Y., Liu, T., & Xu, S. (2015). 2D sequential inversion of total magnitude and total magnetic anomaly data affected by remanent magnetization. *Geophysics*, *80*(3), K1–K12. https://doi.org/10.1190/geo2014-0019.1

Mantovani, M., Louro, V., Ribeiro, V., Requejo, H., & dos Santos, R. (2016). Geophysical analysis of Catalão I alkaline–carbonatite complex in Goiás, Brazil. *Geophysical Prospecting*, *64*(1), 216–227. https://doi.org/10.1111/1365-2478.12283

Nicolosi, I., Blanco-Montenegro, I., Pignatelli, A., & Chiappini, M. (2006). Estimating the magnetization direction of crustal structures by means of an equivalent source algorithm. *Physics of the Earth and Planetary Interiors*, *155*(1-2), 163–169. https://doi.org/10.1016/j.pepi.2005.12.003

Phillips, J. D. (2005). Can we estimate total magnetization directions from aeromagnetic data using Helbig's integrals? *Earth, Planets and Space*, *57*(8), 681–689. https://doi.org/10.1186/BF03351848

Pilkington, M. (1997). 3-D magnetic imaging using conjugate gradients. *Geophysics*, *62*(4), 1132–1142. https://doi.org/10.1190/1.1444214

Pilkington, M., & Beiki, M. (2013). Mitigating remanent magnetization effects in magnetic data using the normalized source strength. *Geophysics*, *78*(3), J25–J32. https://doi.org/10.1190/geo2012-0225.1

Shao, J., Huang, J., Yan, Z., & Liu, Z. (1989). The division and age of basalts in the Nangjing area. *Geological Review*, *35*(2), 97–106. (in Chinese with English abstract)

Shearer, S., & Y. Li (2004), 3D inversion of magnetic total gradient data in the presence of remanent magnetization, *74th* SEG Annual Meeting Expanded Abstracts, 774-777.

Srivastava, S., & Agarwal, B. (2010). Inversion of the amplitude of the two-dimensional analytic signal of the magnetic anomaly by the particle swarm optimization technique. *Geophysical Journal International*, *182*(2), 652–662. https://doi.org/10.1111/j.1365-246X.2010.04631.x

Stavrev, P., & Gerovska, D. (2000). Magnetic field transforms with low sensitivity to the direction of source magnetization and high centricity. *Geophysical Prospecting*, *48*(2), 317–340. https://doi.org/10.1046/j.1365-2478.2000.00188.x

Wang, M., Di, Q., Xu, K., & Wang, R. (2004). Magnetization vector inversion equations and 2D forward and inversed model study. *Chinese Journal of Geophysics*, *47*(3), 528–534. (in Chinese with English abstract)

Wu, H., Zhu, R., Bai, L., Guo, B., & Lü, J. (1998). Revised apparent polar wander path of the Yangtze block and its tectonic implications. *Science in China Series D: Earth Sciences*, *41*, 78–90.

Yang, Z., & Besse, J. (2001). New Mesozoic apparent polar wander path for south China: Tectonic consequences. *Journal of Geophysical Research*, *106*, 8493–8520. https://doi.org/10.1029/2000JB900338

Zhang, X., Wang, H., Wang, Y., Liu, J., & Chen, J. (2016). Application of high-precision aeromagnetic data to expanding prospecting potential of the Yeshan iron deposit. *Geology and Exploration*, *52*(6), 1138–1146. (in Chinese with English abstract)

Zheng, Y., Xiao, W., & Zhao, G. (2013). Introduction to tectonics of China. *Gondwana Research*, *23*(4), 1189–1206. https://doi.org/10.1016/j.gr.2012.10.001

Zhou, J., Meng, X., Guo, L., & Zhang, S. (2015). Three-dimensional cross-gradient joint inversion of gravity and normalized magnetic source strength data in the presence of remanent magnetization. *Journal of Applied Geophysics*, *119*, 51–60. https://doi.org/10.1016/j.jappgeo.2015.05.001

Zhu, R., Yang, Z., Ma, X., Wu, H., Meng, Z., Fang, D., & Huang, B. (1998). Paleomagnetic constraints on the tectonic history of the major blocks of China duing the Phanerozoic. *Science in China Series D: Earth Sciences*, *41*, 1–19.

Journal of Geophysical Research: Solid Earth

Supporting Information for

Extracting induced and remanent magnetizations from magnetic data modeling

Shuang Liu[1,2,3], *Maurizio Fedi*[2], *Xiangyun Hu*[1,*], *Jamaledin Baniamerian*[2,4], *Bangshun Wei*[5], *Dalian Zhang*[5], *and Rixiang Zhu*[3]

[1] *Hubei Subsurface Multi-scale Imaging Key Laboratory, Institute of Geophysics and Geomatics, China University of Geosciences, Wuhan, China*

[2] *Department of Earth, Environmental and Resources Science, University of Naples Federico II, Naples, Italy*

[3] *State Key Laboratory of Lithospheric Evolution, Institute of Geology and Geophysics, Chinese Academy of Sciences, Beijing, China.*

[4] *Department of Earth Sciences, College of Sciences and Modern Technologies, Graduate University of Advanced Technology, Kerman, Iran*

[5] *Geological Survey of Jiangsu Province, Nanjing, China*

[*] *Corresponding author: Xiangyun Hu (xyhu@cug.edu.cn)*

Contents

Section 1. Figures

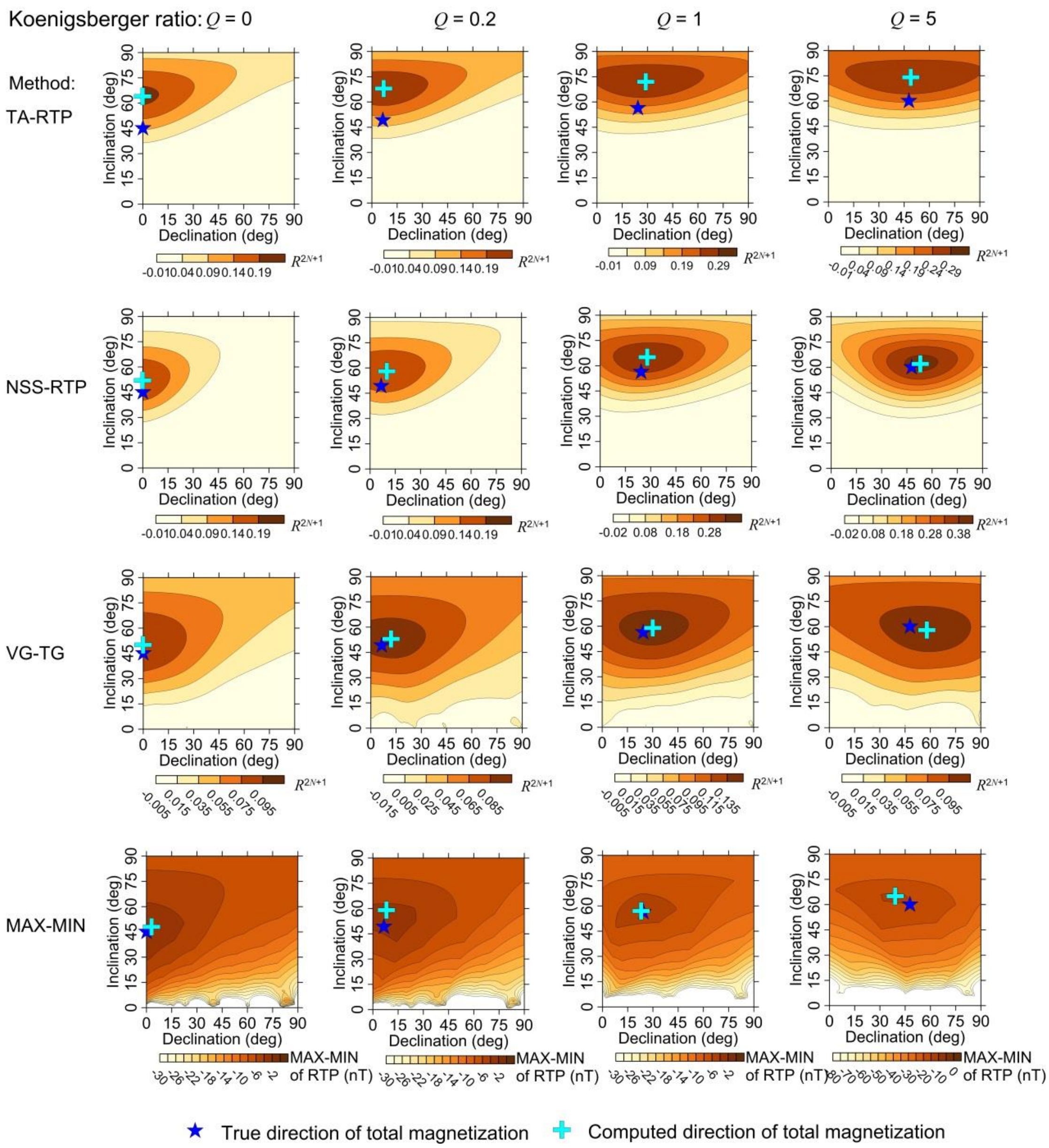

Figure S1 Estimation of the total magnetization direction for the synthetic prism model. Contour maps of TA-RTP, NSS-RTP, VG-TG and MAX-MIN for Q = 0, 0.2, 1 and 5.

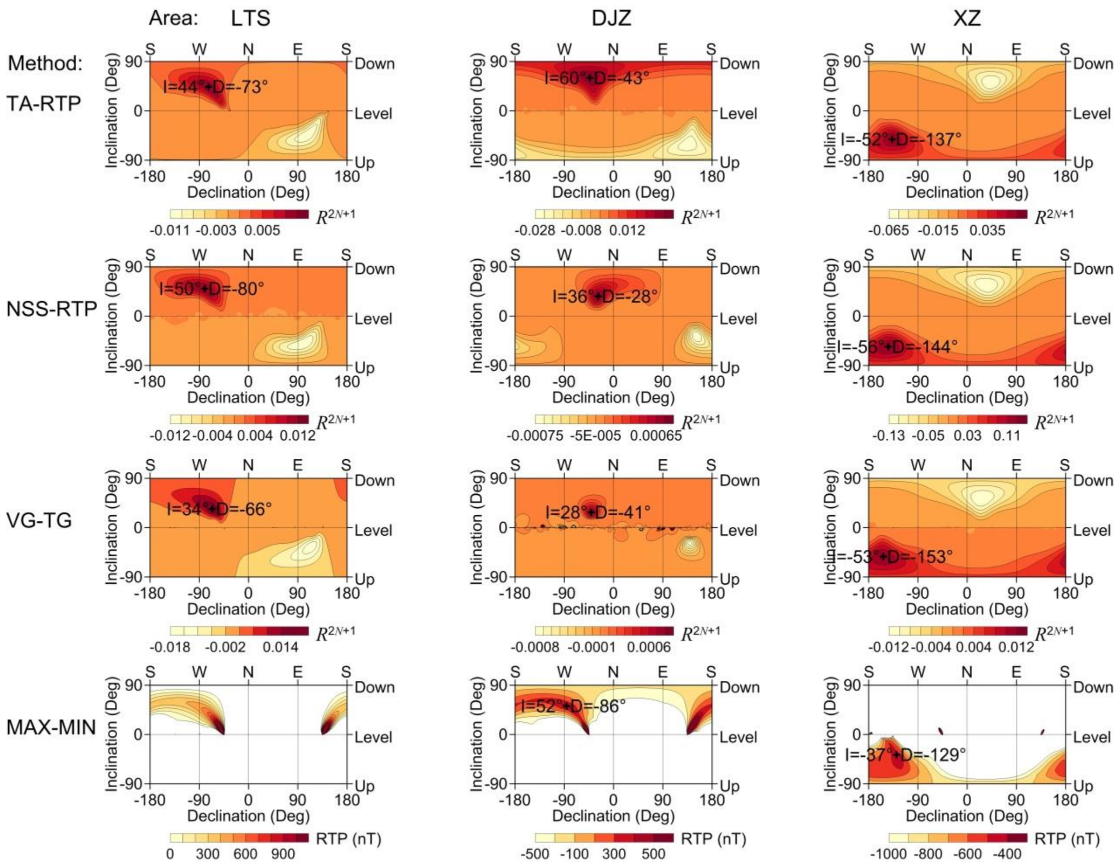

Figure S2 Contour maps of TA-RTP, NSS-RTP, VG-TG and MAX-MIN results to estimate the total magnetization direction for magnetic anomalies of the LTS, DJZ and XZ areas at Yeshan region (eastern China). LTS = Laitoushan; DJZ = Dajingzhao; XZ = Xuezhuang.

Section 2. Tables

Table S1 Geometric and magnetic parameters of synthetic cuboid model with different Koenigsberger ratios when Q = 0, 0.2, 1 and 5.

x_0 (m)		500			
y_0 (m)		500			
z_0 (m)		200			
a (m)		100			
b (m)		200			
c (m)		200			
Geomagnetic field	T_0 (nT)	50000			
	I_0 (deg)	45			
	D_0 (deg)	0			
Koenigsberger ratio Q		0	0.2	1	5
Susceptibility (SI)		0.0126	0.0126	0.0126	0.0126
Induced magnetization	M_i (A/m)	0.5	0.5	0.5	0.5
	I_i (deg)	45	45	45	45
	D_i (deg)	0	0	0	0
Remanent magnetization	M_r (A/m)	0	0.1	0.5	2.5
	I_r (deg)	—	60	60	60
	D_r (deg)	—	60	60	60
Total magnetization	M (A/m)	0.5	0.58	0.95	2.91
	I (deg)	45	49.12	56.27	59.91
	D (deg)	0	6.53	24.34	47.89

Table S2 Computed total magnetization direction and remanent magnetization direction of the synthetic cuboid model when Q = 0, 0.2, 1 and 5.

Koenigsberger ratio Q			0	0.2	1	5
True total magnetization		I (deg)	45	49.12	56.27	59.91
		D (deg)	0	6.53	24.34	47.89
True remanent magnetization		I_r (deg)	—	60	60	60
		D_r (deg)	—	60	60	60
TA-RTP	total magnetization	I (deg)	64	68	72	74
		D (deg)	0	7	29	49
	remanent magnetization	I_r (deg)	—	—	69.32	75.55
		D_r (deg)	—	—	132.87	74.33
NSS-RTP	total magnetization	I (deg)	52	58	65	62
		D (deg)	0	10	28	53
	remanent magnetization	I_r (deg)	—	—	68.87	61.80
		D_r (deg)	—	—	95.08	66.83
VG-TG	total magnetization	I (deg)	50	53	59	58
		D (deg)	0	12	30	58
	remanent magnetization	I_r (deg)	—	34.97 (10.96)	60.76	56.70
		D_r (deg)	—	128.22 (143.51)	76.38	70.61
MAX-MIN	total magnetization	I (deg)	48	59	57	65
		D (deg)	3	8	23	39
	remanent magnetization	I_r (deg)	—	—	61.91	66.75
		D_r (deg)	—	—	58.93	52.03
Averaged (Final)	total magnetization	I (deg)	50	53	60.33	60
		D (deg)	1	12	27	55.5
	remanent magnetization	I_r (deg)	—	34.97 (10.96)	64.49	59.25
		D_r (deg)	—	128.22 (143.51)	75.20	68.67

Table S3 Sensitivity parameters for the synthetic example when Q = 0.2, 1 and 5.

Koenigsberger ratio Q		0.2	1	5
TA-RTP	a	0.9185	0.8636	0.8076
	E	0.8837	1.7458	25.6522
	S_t	—	3.4544	1.3423
	S_Q	—	0.5838	0.0238
	C	—	0.4917	0.7324
	F	—	1.9833	32.3240
	K_Q	—	-0.2895	-0.0298
	K_C	—	-0.1941	-0.0260
NSS-RTP	a	0.9687	0.9047	0.8241
	E	0.9783	1.8185	25.6792
	S_t	—	3.6189	1.3506
	S_Q	—	0.4709	0.0228
	C	—	0.6370	0.7546
	F	—	2.2740	32.5465
	K_Q	—	-0.2763	-0.0296
	K_C	—	-0.1688	-0.0257
VG-TG	a	0.9810	0.9215	0.7982
	E	1.0023	1.8492	25.6372
	S_t	110.3793 (-90.7599)	3.6860	1.3377
	S_Q	20.2438	0.4215	0.0243
	C	0.0468 (-0.4237)	0.6983	0.7199
	F	0.0587 (0.2754)	2.3967	32.1989
	K_Q	-0.2265 (-0.2462)	-0.2713	-0.0299
	K_C	-0.1836 (-0.1295)	-0.1597	-0.0261
MAX-MIN	a	0.9668	0.9475	0.8731
	E	0.9746	1.8978	25.7623
	S_t	—	3.7901	1.3751
	S_Q	—	0.3374	0.0196
	C	—	0.7956	0.8214
	F	—	2.5913	33.2142
	K_Q	—	-0.2638	-0.0291
	K_C	—	-0.1469	-0.0250

Table S4 Magnetic property measurements for rock and ore samples of the Yeshan region (eastern China). *Ns* = number of samples.

Rocks and ores	*Ns*	κ (SI)		M_r (A/m)		M_i (A/m)		*Q*	Occurred area
		Range	Mean	Range	Mean	Range	Mean		
Magnetite	9	0.33-2.38	1.17	3.7-29.6	14.6	13-94.5	46.6		
Mineralized skarn	8	0.022-0.1	0.055	0.41-2.45	1.2	0.85-3.85	2.23		
Mineralized gabbro	63	0.019-0.11	0.037	0.1-4.29	1.17	0.73-4.5	1.46		
Mineralized marble	7	0.14-0.62	0.27	0.94-8.75	2.19	5.4-24	10.7		
Alterated diorite	123	0-0.032	0.007	0-2.14	0.14	0-1.25	0.28	0.5	LTS
Alterated syenite	55	0-0.018	0.0078	0-0.64	0.18	0-0.71	0.31	0.6	LTS
Granodiorite	12	0.0063-0.039	0.011	0.01-0.73	0.27	0.25-1.53	0.45	0.6	LTS, DJZ
Monzonite	18	0.001-0.016	0.0044	0.05-0.48	0.2	0.04-0.6	0.17	1.2	LTS, DJZ
Dioritic porphyrite	14	0-0.034	0.0082	0-7.22	1.39	0-1.35	0.32	4.3	DJZ
Basalt	117	0-1.032	0.029	0-232	6.67	0-41.05	1.18	5.7	XZ
Trachy basalt breccia lava	16	0.041-0.099	0.072	0.12-11.86	1.57	1.61-3.9	2.7		
Trachy basalt breccia	64	0-0.09	0.018	0-10.4	0.46	0-3.6	0.69		
Trachy basalt	75	0.029-0.091	0.048	0-7.6	0.76	1.1-3.6	1.9		
Alterated trachy basalt	67	0.048-0.12	0.068	0-5.34	0.74	1.9-4.7	2.7		
Andesite	54	0-0.24	0.028	0-32.77	1.85	0-9.6	1.1		
Mica gabbro	8	0.0041-0.023	0.01	0.17-2.71	0.47	0.16-0.9	0.4		
Diabase	8	0.003-0.013	0.0054	0.43-1.2	0.78	0.12-0.53	0.21		
Biotite pyroxene diorite	192	0.0057-0.1	0.031	0.45	—	—	—		
Quartzite	14	0	0	0	0	0	0		
Limestone and dolomite	69	0	0	0	0	0	0		

Table S5 Computed total magnetization direction and remanent magnetization direction of the LTS, DJZ and XZ areas at Yeshan region (eastern China). LTS = Laitoushan; DJZ = Dajingzhao; XZ = Xuezhuang.

Area		LTS	DJZ	XZ
Koenigsberger ratio *Q*		0.8	1.0	5.7
Total magnetization of TA-RTP	*I* (deg)	44	60	-52
	D (deg)	-73	-43	-137
Total magnetization of NSS-RTP	*I* (deg)	50	36	-56
	D (deg)	-80	-28	-144
Total magnetization of VG-TG	*I* (deg)	34	28	-53
	D (deg)	-66	-41	-153
Total magnetization of MAX-MIN	*I* (deg)	—	—	-37
	D (deg)	—	—	-129
Final total magnetization	*I* (deg)	42.7 ±8.1	32 ±5.7	-53.7 ±2.1
	D (deg)	-73 ±7.0	-34.5 ±9.2	-144.7 ±8.0
Final remanent magnetization	I_r (deg)	-3.0 ±31.6 (-40.9 ±3.3)	10.6 ±20.2	-54.0 ±1.5
	D_r (deg)	-122.2 ±27.3 (-163.0 ±2.9)	-53.3 ±32.6	-152.0 ±5.6
Sensitivity parameters	*a*	0.6975	0.8866	-0.9320
	E	1.1265	1.7861	33.3587
	S_t	3.8981 (-0.4106)	3.5466	0.6977
	S_Q	2.5183 (-0.9518)	0.5216	0.0112
	C	-0.3323 (-0.9518)	0.5722	-0.9320
	F	0.1083 (-0.8828)	2.1443	21.8647
	K_Q	-0.4008 (3.7846)	-0.2820	-0.0436
	K_C	-0.6857 (-19.9485)	-0.1794	-0.0521
VGP	λ_p (°N)	27.3 (72.0)	33.2	66.8
	φ_p (°E)	226.7 (238.6)	371.4	198.4

Table S6 Comparisons of remanent magnetization directions and VGP between this study and previous work for basalt rocks at XZ area. XZ = Xuezhuang , XPS = Xiaopanshan; LYS = Lingyanshan; FS = Fangshan; PS = Pingshan; R = Reversed geomagnetic polarity; N = Normal geomagnetic polarity; *Ns* = Number of samples; λ_p, φ_p = the latitude and longitude of the VGP.

Authors	Sampling place	*Ns*	I_r (deg)	D_r (deg)	λ_p (°N)	φ_p (°E)	Polarity
This study	XZ	—	-54.0	-152.0	66.8	198.4	R
Shao et al. (1989)	XPS	41	-43.0	-179.6	82.5	296.0	R
Liu et al. (1976)	LYS	5	42.2	354.7	80.6	330.0	N
	FS	13	-54.15	-164.5	76.8	182.4	R
Cheng et al. (1991)	FS	12	-55.5	158.4	71.8	14.8	R
	PS	10	42.9	18.6	72.1	227.9	N

Section 3. Data (Files uploaded separately)

Date Set S1: jgrb53105-sup-0002-2017JB015364_ds01.grd, magnetic data of Figure 2a (synthetic example)

Date Set S2: jgrb53105-sup-0002-2017JB015364_ds02.grd, magnetic data of Figure 2b (synthetic example)

Date Set S3: jgrb53105-sup-0002-2017JB015364_ds03.grd, magnetic data of Figure 2c (synthetic example)

Date Set S4: jgrb53105-sup-0002-2017JB015364_ds04.grd, magnetic data of Figure 2d (synthetic example)

Date Set S5: jgrb53105-sup-0002-2017JB015364_ds05.grd, magnetic data of Figure 7 (field example)

*.grd file format: GRD Surfer 6 text Grid.